

## Invited Article

# Pressure induced physical variations in the lead free fluoropervoskites $XYF_3$ (X=K, Rb, Ag; Y=Zn, Sr, Mg): Optical materials

Shakeel<sup>a</sup>, Ali H. Reshak<sup>b,c,\*</sup>, Shamim Khan<sup>d</sup>, A. Laref<sup>e</sup>, G. Murtaza<sup>d,f</sup>, J. Bila<sup>c</sup>

<sup>a</sup> Department of Physics, Qurtuba University of Science & Information Technology, Pakistan

<sup>b</sup> Physics Department, College of Science, Basrah University, Basrah, Iraq

<sup>c</sup> Department of Instrumentation and Control Engineering, Faculty of Mechanical Engineering, CTU in Prague, Technicka 4, Prague, 6166 07, Czech Republic

<sup>d</sup> Materials Modelling Lab, Department of Physics, Islamia College University, Peshawar, Pakistan

<sup>e</sup> Department of Physics and Astronomy, College of Science, King Saud University, Riyadh, 11451, Saudi Arabia

<sup>f</sup> Department of Mathematics & Natural sciences, Prince Mohammad Bin Fahd University, P. O. Box 1664, Alkhobar 31952, Saudi Arabia



## ARTICLE INFO

## Keywords:

Fluoro-perovskites  
Energy gaps  
Pressure effects  
Interband transitions  
Optical materials

## ABSTRACT

The optical and electronic properties of fluoro-perovskites  $XYF_3$  (X = K, Ag, Rb; Y=Zn, Sr, Mg) were investigated under pressure ranging from 0 to 50 GPa, utilizing full potential method based on density functional theory (DFT). The generalized gradient approximation GGA-PBE and GGA-PBESol functional are used for calculating the structural properties while TB-mBJ functional is employed for the calculation of optical and electronic properties. The lattice constant increases by varying the cation from Zn to Mg to Sr. The volume-ratios as a function of pressure reveal that  $AgZnF_3$  has a low compressibility among the whole series of these compounds. At zero pressure, all these compounds exhibit indirect wide bandgap. The band gap of  $AgMgF_3$ ,  $KMgF_3$ ,  $KZnF_3$ ,  $RbMgF_3$  and  $RbZnF_3$  increases with pressure, while that of  $AgZnF_3$  and  $KSrF_3$  first increases with rising the pressure from zero to 10 Gpa for  $AgZnF_3$  and from zero to 5 Gpa for  $KSrF_3$  and then, decreases smoothly with increasing the pressure up to 50 GPa. The band gap type of  $RbSrF_3$  and  $KSrF_3$  change from indirect to direct at a pressure of 5 GPa and 40 Gpa, respectively. The high pressure shows significant influence on the density of states; it reduces and shift the highest peaks towards negative energy with broader bandwidths. The electron density plots explored a mixed covalent as well as ionic bonding at zero pressure. The covalent bonding becomes stronger under high pressure. The optical conductivity, refractive index and reflectivity spectra reveal a blue shift with the rise in pressure, due to rise in the band gap and the broadening of bands with compression.

## 1. Introduction

The solids which have a similar kind of crystal structure as  $CaTiO_3$  are called Perovskites. These solids were named for a mineralogist, Count Lev Aleksovich von Peroski, found in 1839 and entitled by Gustav Rose while investigating the samples discovered in the Ural Mountains [1]. Fig. 1 shows the fundamental cubic structure of perovskites with general formula  $ABX_3$ , here A represents the alkali metal, B represents the transition metal or a lanthanide or alkaline metal, and X is for either a halogen group element or oxygen (O, F, Br, I, Cl).

Perovskites display very interesting physical and chemical properties, therefore, these materials are used in an extensive variety of applications, for example, memory gadgets, sensors, solid-state proton detectors, auto exhaust catalysts, piezoelectric transducers etc. Fluoride

perovskites ( $ABF_3$ ) are critical due to their fascinating structural and physical properties like photoluminescence [2,3], piezoelectricity [4], ferroelectricity [5], semi conductivity [6], anti-ferromagnetism [7], optical properties [8–10]. These materials have been utilized in optical applications, magnetic tunnel junctions, power storage, semiconductors, lenses and medical applications [11–13].

Much attention-grabbing questions in planetary and geophysics, in addition to applied science, are related to the physical properties of materials at high pressure. Pressure, as an interesting thermodynamic variable, gives an amazing way to investigate the electronic and structural compartments of solid state materials. Applying pressure on materials can cause to decrease the interatomic distances and to a close packing factor, which would strongly alter the electronic orbitals and bonding patterns [14–17]. Also, due to the effect of high pressure, most

\* Corresponding author. Physics Department, College of Science, Basrah University, Basrah, Iraq.

E-mail address: [maalidph@yahoo.co.uk](mailto:maalidph@yahoo.co.uk) (A.H. Reshak).

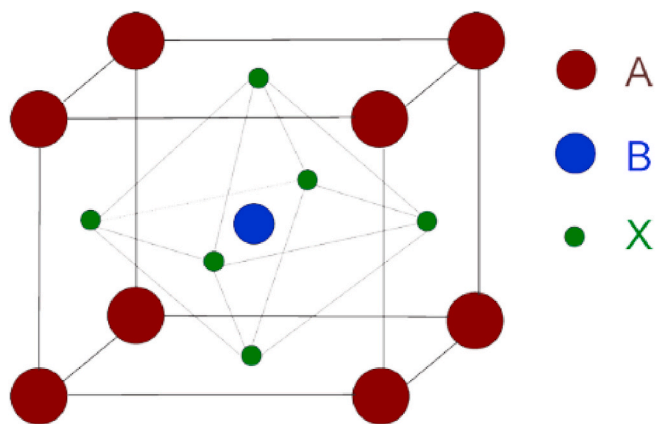


Fig. 1. The crystal structure of perovskite with  $ABX_3$  formula.

materials become unstable and shift into new phases with an increase in densities. In recent years, numerous materials with new crystal structure types have been noticed at high pressure via experiments and computational analysis [18]. These structures are frequently novel and occasionally not reported at normal atmospheric pressure. It has been discovered that these new crystal structures can have assortment of electronic states, i.e. superconducting, metallic, super-ionic, or super-hard states. These revelations are of great interests in technological applications and to understand the physics of electronic processes in compounds, for example, chemical bonding. Numerical simulations have eased the investigation of physical properties of high pressure solids.

Numerous experimental as well as theoretical research publication were dedicated to the investigations of perovskites. The cubic perovskite structure  $ABX_3$  displays a longer A–X separation than the B–X. Their configuration is connected to the temperature, pressure and chemical composition [19]. Studies have revealed that the space group of cubic perovskites is  $Pm-3m$  (#221) as displayed in Fig. 1, where each B cation is bordered by 6 anions (X), while the each A cations are bordered by 12 anions (with coordination number is 12). The anions (X) are bordered by 2 cations (B cations), since the bond length of A–X is greater than the B–X [20].

In experiments, it is very difficult to reach and control high pressure in diamond anvil cells. Despite what might be expected, changing pressure in computational calculations can be proficient clearly by changing the unit cell size. With the quick improvements of computational power and software, theoretical investigations of materials at high pressure had flourished in the course of recent decades. The research on the complexities of the solids and the correctness (accuracy) in which physical properties can be anticipated, have increased quickly throughout the years. The first principles methods have performed a critical role in investigating and controlling analysis at high pressure. Computational physics have been built up as an important tool in collaboration with the investigations at high pressure. Alternatively, new experimental work at high pressure keep on giving a challenging test to both theory and computational methods.

Cui et al., [21] made a theoretical investigation on  $KMgF_3$  in the framework of density functional theory (DFT) and observed that  $KMgF_3$  have an indirect band gap insulator in the pressure range 0–100 GPa. Sahli et al. [22], conducted theoretical research on the mechanical, electronic, optical and structural properties of  $KMgF_3$  fluoride perovskite under hydrostatic pressure up to 10 GPa and utilized FP-(L)APW + lo method established on DFT. They used various functionals, particularly GGA-PBEsol for the computation of elastic and structural properties, and TB-mBJ for optical and electronic properties. They discovered that the elastic and structured parameters were in good agreement with the accessible experimental results, calculated by GGA-PBEsol and Mehl model, respectively. Vaitheeswaran et al. [23], reported a high pressure

(0–40 GPa) investigation on  $KMgF_3$ , utilized the full-potential linear muffin-tin orbital (FP-LMTO) technique, established on DFT. They classified  $KMgF_3$  as brittle solid and extremely stable at high pressure. They addressed that the band gap calculated with LDA was 6.95 eV.

Larbi et al. [24], investigated the behavior of the electronic and structural properties of  $RbZnF_3$  under the influence of pressure (0–10 GPa), by utilizing the FP-LAPW technique. They used GGA-PBE and GGA-PBEsol functionals, as executed in the Wien2k code. They found that the calculated bulk modulus was close to reported literature, they also addressed that  $RbZnF_3$  possessed an indirect band gap and this band nature remains the same under the impact of pressure (up to 10 GPa).

Aguado et al. [25], experimentally investigated the structural stability of  $KXF_3$  (X: Mg, Zn, Co, Ni) utilizing X-ray diffraction techniques under pressure ranging 0–10 GPa. They found that  $KZnF_3$  is stable in the studied range of pressure, while  $KMF_3$  compounds is structurally stable up to 50 GPa. Meziani et al. [26], theoretically calculated the elastic, optical, electronic and structural properties of  $KZnF_3$  by utilizing FP-LAPW technique based on DFT. They analyzed the behavior of the band structure under the effect of pressure. Their result indicates that the band gap increased linearly with increasing the pressure.

From the literature review, it is pretty clear that no theoretical and experimental work is available in the existing literature for  $AgSrF_3$  compound. Some work has been performed on  $XYF_3$  (X = K, Rb, Ag; Y = Zn, Sr, Mg) compounds individually, related to their structural, electronic, optical and elastic properties, utilizing ab initio technique.  $KMgF_3$  compound is investigated theoretically under high pressure (0–40 GPa),  $KZnF_3$  and  $RbZnF_3$  are also studied under pressure range (0–10 GPa). However, no experimental and theoretical investigation is performed on the whole series of these compounds ( $XYF_3$ ) under the impact of high pressure (up to 50 GPa).

In this work, we aim at revealing and understanding the structural, optical and electronic properties under high pressure ranging from 0 to 50 GPa by conducting and analyzing the first-principles calculations on  $XYF_3$  (X = K, Rb, Ag; Y = Zn, Sr, Mg) fluoroperovskites. We also discussed in great detailed the band gap behavior of these compounds under high pressure.

## 2. Computational details

The physical properties of the compounds have been explored by putting into use the all electron FP-LAPW method as utilized in the Wien2K package [27]. To carry out the electronic structure calculations in the framework of DFT, we determine the solution of the Kohn-Sham equation.

$$\left( -\frac{1}{2}\nabla^2 + V_{\text{eff},\sigma}^{\text{KS}}(r) \right) \psi_{i,\sigma}(r) = \epsilon_{i,\sigma} \psi_{i,\sigma}(r) \quad (1)$$

where,  $\psi_{i,\sigma}$  is the single electron wave function and  $V_{\text{eff},\sigma}^{\text{KS}}$  is Kohn-Sham multiplicative effective Potential which is equal to  $V_{\text{eff},\sigma}^{\text{KS}} = V_{\text{ext}} + V_{\text{H}} + V_{\text{xc},\sigma}$  i.e. sum of the external Hartree and the Exchange-correlation term and  $\sigma$  represents the spin of electron. In the Kohn Sham formalism all terms are exact except the exchange-correlation potential which have to be approximated. The well-known exchange correlations potentials are the local density approximation (LDA) [28] and the generalized gradient approximations (GGA) [29]. However, these potentials underestimate the electronic band structure that's why other potentials involving the higher order gradients were proposed to study the band structure. The main drawback in GGA and also in LDA is because of  $\nabla_{\text{xc}}$  is zero. To overwhelm this imperfection, mostly the method of Becke and Johnson is used [30]. Tran and Blaha added a parameter intending to alter the relative weight of the two terms in BJ potential. At a later time, it is known as modified Becke-Johnson (mBJ) [31] exchange potential approximation. To be briefly it is written as TB-mBJ. Mathematically, the TB-mBJ is given as;

$$V_{xc,\sigma}^{mBJ}(r) = cV_{xc,\sigma}^{BR}(r) + (3c-2)\frac{1}{\pi}\sqrt{\frac{5}{12}}\sqrt{\frac{2t_{\sigma}(r)}{\rho_{\sigma}(r)}} \quad (2)$$

The original BJ potential can be obtained again when  $c = 1$ . Where  $c$  is given as

$$c = \alpha + \beta \left( \frac{1}{V_{cell}} \int d^3r \frac{|\nabla \rho(r)|}{\rho(r)} \right)^{1/2} \quad (3)$$

where,  $V_{cell}$  represents unit cell volume. Similarly,  $\alpha$  and  $\beta$  represents unbound terms in comparison with the experimental results. Therefore, by use of value of  $c$ , the results of the band gap enhanced and satisfactory for small and wide bandgap materials.

Muffintin radii (Rmt) of the ions in the spherical region are chosen in such a way that no charge leakage take place. Rmt\*Kmax, which determines the number of basis functions (size of the matrices) was set to 7. Rmt is the smallest radii value of any atomic sphere and Kmax is the highest value of the plane wave cut off. A suitable value of 1000 k-points were used for the Brilluion zone integrations. In the crystal structure of  $XYF_3$  (X = K, Rb, Ag; Y = Zn, Sr, Mg), X cation occupy the (0, 0, 0) position, Y cations resides at the center of the cell (0.5, 0.5, 0.5) and anion F anion settle at the face centers of the cell (0.5, 0.5, 0)

### 3. Results and discussion

#### 3.1. Structural properties

Foremost, we targeted to find the optical and electronic properties under the impact of a high pressure ranging from 0 to 50 GPa. This

investigation can be done by finding the stability of the considered materials under high pressure range (0–50 GPa), which needs details of the structural parameters, for example, the pressure derivative of bulk modulus, bulk modulus, and lattice parameters. In this way, using the lattice constant from the equation of state to figure out the optical and electronic properties under the impact of a high pressure up to 50 GPa.

To investigate the structural properties of  $XYF_3$  (X = K, Rb, Ag; Y = Zn, Sr, Mg), the volume optimization method is executed by minimization of the unit cell energy verses the unit cell volume and it is fit in the Murnaghan's equation of state [27] as depicted in Fig. 2. These figures present that by decreasing the volume of the unit cell, the unit cell energy decreases and reaches to the minimum unit cell energy. This minimum energy is designated as ground state energy, the optimum volume is the volume of that system having minimum energy (ground state energy). By further increase in the volume of the unit cell the energy of the unit cell rises and the system becomes unstable. The lattice constants,  $a_0$ , the bulk moduli,  $B_0$ , pressure derivative of bulk modulus,  $B'$  of  $XYF_3$  (X = K, Rb, Ag; Y = Zn, Sr, Mg) are assessed at the optimum volume and given in Table 1. In the calculation of structural properties, we have used two functionals GGA-PBE as well as GGA-PBESol. The results of GGA-PBESol is outstanding in the calculation of structural properties of condensed materials and endorsed by several preceding works [28–30]. It is a modified approach of GGA-PBE potential which mostly advances the accuracy of the materials structural properties.

Accounting for the structural properties of these materials, we studied the lattice constant calculated by using GGA-PBE and also GGA-PBESol functionals, the lattice constant obtained by GGA-PBE is overestimated in comparison with the existed experimental results. Whereas, GGA-PBESol significantly diminishes this overestimation and the

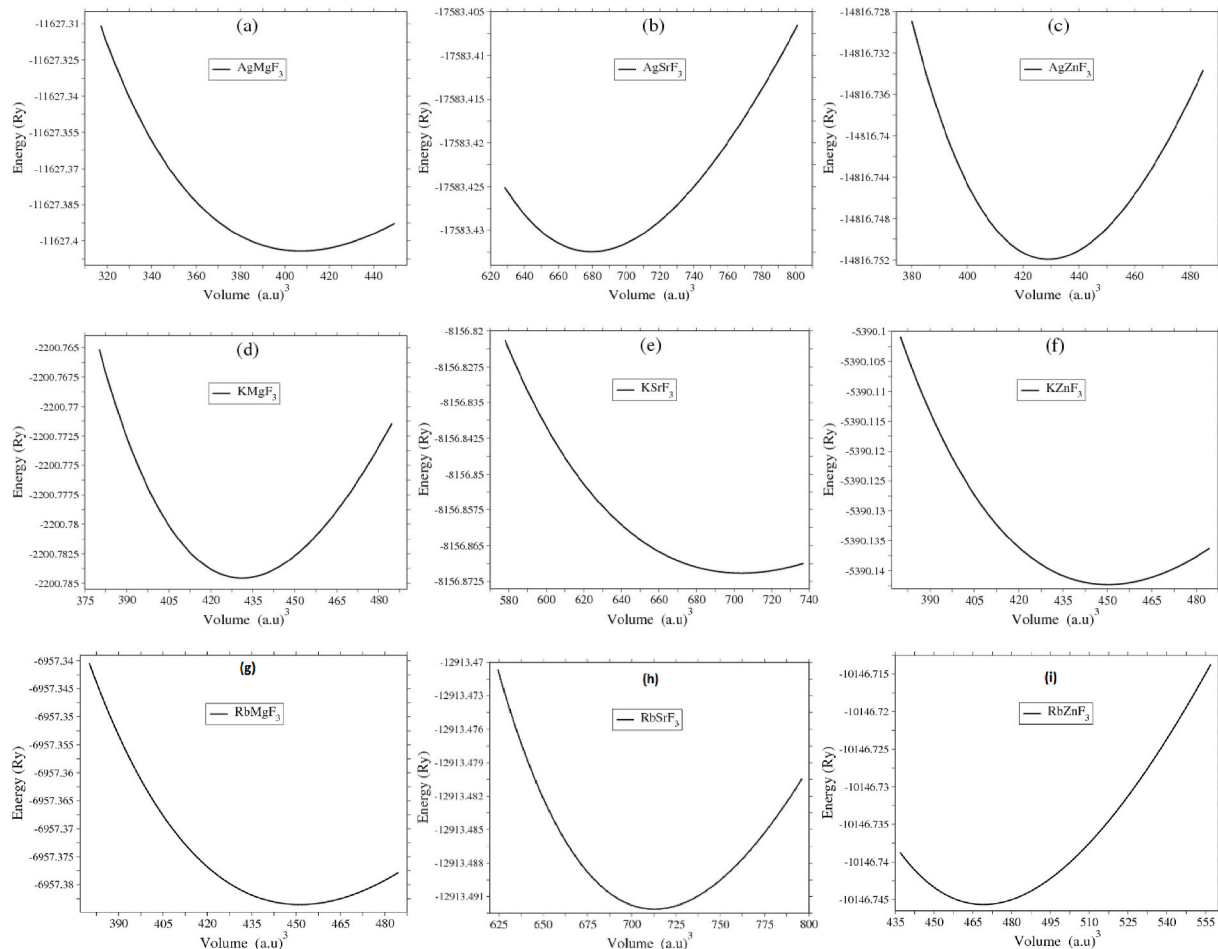


Fig. 2. Unit cell energy versus unit cell volume of  $AgMgF_3$ ,  $AgSrF_3$ ,  $AgZnF_3$ ,  $KMgF_3$ ,  $KSrF_3$ ,  $KZnF_3$ ,  $RbMgF_3$ ,  $RbSrF_3$  and  $RbZnF_3$ , respectively.

**Table 1**

Calculated lattice constant,  $a_0$  (in Å), bulk modulus,  $B_0$  (in GPa), pressure derivative of bulk modulus,  $B'$  and ground state energy  $E_0$  (in Ry) of AgMgF<sub>3</sub>, AgSrF<sub>3</sub>, AgZnF<sub>3</sub>, KMgF<sub>3</sub>, KSRF<sub>3</sub>, KZnF<sub>3</sub>, RbMgF<sub>3</sub>, RbSRF<sub>3</sub>, and RbZnF<sub>3</sub>, compared with the theoretical and experimental results.

	$a_0$ (Å)	$B_0$ (GPa)	$B'$	$E_0$ (Ry)
<b>AgMgF<sub>3</sub></b>				
This work	3.998 (PBE)	69.5570	5.0000	-11635.056096
	3.922 (PBEsol)	89.3392	3.9867	-11627.404103
Experimental work	3.920 [44], 3.918 [45]	-	-	-
Other work	3.885 [46], 3.724 [47], 3.982 [48], 3.724 [47]	98.088 [46]	5.0000 [46]	-11632.4003 [46]
<b>AgSrF<sub>3</sub></b>				
This work	4.740 (PBE)	43.4016	5.0000	-17594.062947
	4.652 (PBEsol)	48.0072	5.0000	-17583.432452
Experimental work	-	-	-	-
Other work	-	-	-	-
<b>AgZnF<sub>3</sub></b>				
This work	4.071 (PBE)	80.2431	5.0298	-14826.346370
	3.991 (PBEsol)	95.1249	5.0000	-14816.751946
Experimental work	3.970 [44], 3.972 [45]	-	-	-
Other work	3.953 [46], 3.955 [49], 4.007 [48], 3.743 [49]	77.574 [50], 92.412 [50]	4.747 [50], 4.956 [50]	-14823.1583 [46]
<b>KMgF<sub>3</sub></b>				
This work	4.068 (PBE)	59.2569	5.0000	-2204.990070
	3.997 (PBEsol)	73.2539	5.0000	-2200.784549
Experimental work	3.973 [51], 3.993 [52], 3.9839 [53]	71.200	-	-
Other work	3.999, 4.0644 [22]	-	-	-
<b>KSRF<sub>3</sub></b>				
This work	4.777 (PBE)	39.2963	5.0000	-8164.046449
	4.707 (PBEsol)	43.1262	5.0000	-8156.870755
Experimental work	-	-	-	-
Other work	4.61, 4.77 [54],	-	-	-
<b>KZnF<sub>3</sub></b>				
This work	4.134 (PBE)	71.6021	5.0000	-5396.290408
	4.056 (PBEsol)	79.2033	5.0000	-5390.142353
Experimental work	4.054 [55], 4.056 [56]	77.6 [57]	-	-
Other work	4.05 [44], 4.1352 [50], 4.0589 [50]	68.020 [50], 77.214 [50]	4.685 [50], 4.371 [50]	-
<b>RbMgF<sub>3</sub></b>				
This work	4.142 (PBE)	67.2234	5.0000	-6963.686018
	4.059 (PBEsol)	79.7023	5.0000	-6957.383560
Experimental work	-	-	-	-
Other work	-	-	-	-
<b>RbSRF<sub>3</sub></b>				
This work	4.796 (PBE)	39.3682	4.7626	-12922.771921
	4.727 (PBEsol)	43.8372	5.0000	-12913.492138
Experimental work	-	-	-	-
Other work	-	-	-	-
<b>RbZnF<sub>3</sub></b>				
This work	4.195 (PBE)	62.0892	5.0000	-10154.992545
	4.112 (PBEsol)	79.3490	5.0000	-10146.745661
Experimental work	4.122 [49], 4.11 [44]	-	-	-
Other work	3.900 [45]	86.92 [45]	-	-

calculated lattice constant values are very close to that of experimental values.

The absolute cohesive energy and high bulk modulus show high crystal rigidity. Therefore, we can accept that AgZnF<sub>3</sub> is less

compressible and harder than the other compounds based on  $B_0$  values as shown in Table 1. AgSrF<sub>3</sub> is more compressible than AgZnF<sub>3</sub> because of the lattice constant. Those compounds which have large lattice constant are more compressible as compare to those of having a smaller lattice constant. Those compounds which contain Sr are soft and more compressible as compared to the compounds containing Zn.

Using the optimized data at zero pressure, we can calculate the lattice parameters of these compounds under the influence of high pressure, with the help of following equation [31].

$$a(P) = a_0 \left[ 1 + P \frac{B'}{B_0} \right]^{-\frac{1}{3B'}} \quad (4)$$

where P represents the hydrostatic pressure,  $B_0$  and  $B'$  represents the bulk modulus and pressure derivative of the bulk modulus respectively, and  $a_0$  represents equilibrium lattice parameter.

A number of theoretical studies have conformed the effectuality of this equation [32–34] for forecasting the lattice constant under the impact of pressure and on other different physical properties. So as to clear up the impact of pressure on the structures, the pressure dependent lattice parameter ratios ( $a/a_0$ ) and volume ratios ( $V/V_0$ ) ( $a_0$  and  $V_0$  denote the parameters at zero pressure) are displayed in Fig. 3. By comparing the pressure dependent volume ratios  $V/V_0$  curves (Fig. 3a), we can easily find that KSRF<sub>3</sub>, RbSRF<sub>3</sub> and AgSrF<sub>3</sub> are more easily compressed due to large decrease in the volume. In AgZnF<sub>3</sub> compound the compressibility is low which indicates high hardness AgMgF<sub>3</sub>, RbZnF<sub>3</sub>, RbMgF<sub>3</sub> and KZnF<sub>3</sub> shows similar compressibility. The structural analysis shows that one can modify the compressibility of compounds, as the compressibility of RbSRF<sub>3</sub> compound is larger, one can reduce the compressibility by replacing Sr with Zn and Rb with Ag respectively. The compressibility of those compounds having Mg is greater than AgZnF<sub>3</sub> and lower than RbSRF<sub>3</sub>.

### 3.2. Electronic properties

#### 3.2.1. Band structure

The nine perovskites XYF<sub>3</sub> (X = K, Rb, Ag; Y = Zn, Sr, Mg) studied in present work with calculated band gaps at zero ambient pressure are presented in Table 2. All these un-pressed compounds are indirect band gap insulators.

The changes in the band gap values of these compounds are calculated under high pressure and plotted in Fig. 4. The band gap type of AgMgF<sub>3</sub>, AgSrF<sub>3</sub>, AgZnF<sub>3</sub>, KMgF<sub>3</sub>, KZnF<sub>3</sub>, RbSRF<sub>3</sub> and RbZnF<sub>3</sub> compounds remains indirect in the whole range of studied pressure. We observed the indirect-direct band gap transition in KSRF<sub>3</sub> and RbMgF<sub>3</sub> compounds at about 5 GPa and 40 GPa, respectively and then remains direct up to 50 GPa. Fig. 4 depicts that for KMgF<sub>3</sub> and RbMgF<sub>3</sub>, the band gap monochromatically increases as the pressure increases in the range 0–40 GPa, and from 40 to 50 GPa the band gap remains constant. The band gap of RbZnF<sub>3</sub>, and KZnF<sub>3</sub> increase while the band gap of KSRF<sub>3</sub>, AgSrF<sub>3</sub> and AgZnF<sub>3</sub> decrease as the pressure increases. In case of RbSRF<sub>3</sub> and AgMgF<sub>3</sub>, as the pressure increase from zero to 25 GPa the band gap increases while the band gap decreases in the pressure range from 25 GPa to 50 GPa.

The reasons behind the indirect to direct band structure transitions of KSRF<sub>3</sub> is very closely related to the fact of the material compressibility under pressure. This decisively depends on the energy up-shifting or down shifting of the k-symmetric points at valence band maximum (VBM) or conduction band minimum (CBM) under pressure, which results from the hybridization states. Fig. 4 shows the valence band structure at zero and 5 GPa pressure of KSRF<sub>3</sub>. The analysis of the band structure diagram of KSRF<sub>3</sub> shows that the CBM lies on  $\Gamma$  point where the VBM lies on the R point at zero pressure. By increasing the pressure up to 5 GPa, the energy of the states up-shifts in the valence band at  $\Gamma$  point while in the conduction band the energy of the states down-shifts at point  $\Gamma$  point resulting in the indirect-direct band structure transition.

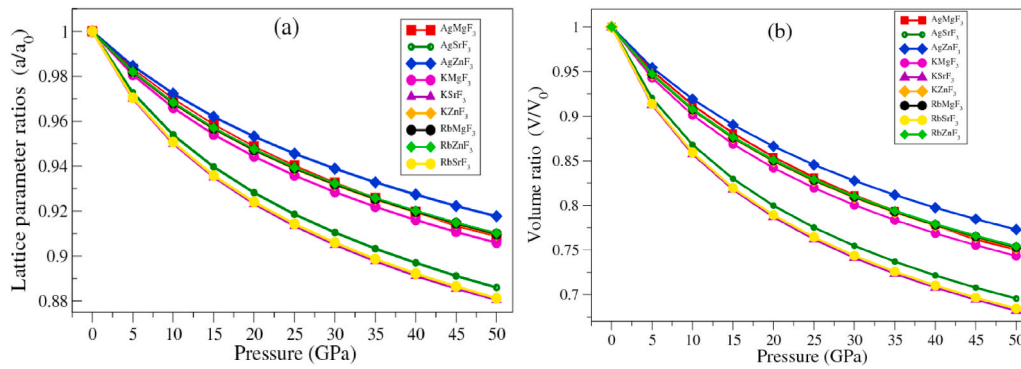


**Fig. 3.** (a) Pressure dependent volume ratio ( $V/V_0$ ) and (b) pressure dependent lattice parameter ratios ( $a/a_0$ ) (note:  $a_0$ ,  $c_0$  and  $V_0$  denote the parameters at zero pressure). Calculated within GGA-PBEsol.

**Table 2**

The calculated band gap energy (in eV) at zero ambient pressure of  $XYF_3$  ( $X = K, Rb, Ag; Y = Zn, Sr, Mg$ ) compounds using TB-mBJ functional, the values are compared with the experimental and other theoretical work.

Compounds	This work (eV)	Other theoretical work (eV)	Exp. work	Band structure type
AgMgF <sub>3</sub>	5.09	0.78 [46]	-	Indirect
AgSrF <sub>3</sub>	6.32	-	-	Indirect
AgZnF <sub>3</sub>	4.66	0.75 [46] (4.851, 1.644, 1.350, 1.501) [50]	-	Indirect
KMgF <sub>3</sub>	10.91	1.31 [11], 7.27 [11], 7.8 [9]	12.4 f [58]	Indirect
KSrF <sub>3</sub>	10.38	5.30 [11] (10.35, 5.54, 5.42) [54]	-	Indirect
KZnF <sub>3</sub>	6.96	3.91 [11] (7.237, 3.721, 4.66, 3.727) [50]	-	Indirect
RbMgF <sub>3</sub>	10.53	7.32 [11]	-	Indirect
RbSrF <sub>3</sub>	9.92	5.60 [11]	-	Indirect
RbZnF <sub>3</sub>	6.81	7.2 [59]	-	Indirect

Because at  $\Gamma$  point, bond Sr-F has mixed covalent and ionic nature while at R point the bond K-F is purely ionic. With the pressure the covalent bonding nature at  $\Gamma$  point changes more as compare with the ionicity of the bonding at the R point [35]. We can further explain this

phenomenon as the VBM at symmetric point  $\Gamma$  has some antibonding hybrid states of F- $p$  states and Sr- $p$  orbitals in KSrF<sub>3</sub>, by applying high pressure the lattice constant contracts which result in to increase the amount of overlap between these orbitals. Due to this increase in the overlap the energies of the states upshift at higher symmetry point  $\Gamma$  of the first Brillouin zone. This upshift in the energy of the states is responsible for the indirect-direct band transitions in KSrF<sub>3</sub> compound. The same explanation is hold for the RbMgF<sub>3</sub> compound, the VBM at point  $\Gamma$  is consists of the antibonding states of F- $p$  states and Mg- $f$  and Mg- $d$  states.

Fig. 4 shows that the band gap energy ( $E_g$ ) of KSrF<sub>3</sub>, AgSrF<sub>3</sub> and AgZnF<sub>3</sub> diminish with pressure. The investigation of the band structures of KSrF<sub>3</sub> (Fig. 6c and d), AgSrF<sub>3</sub> (Fig. 5c and d) and AgZnF<sub>3</sub> (Fig. 5e and f) clearly shows that the bands are dispersed with pressure. This impact of pressure is unsurprisingly a direct result of volume contraction which rise the overlap between the neighboring orbitals which is responsible for the escalation in the electronic band dispersion. These bands comprise of antibonding, bonding and nonbonding orbitals. By applying pressure, the overlap between these orbitals increase, the antibonding nature of the bands pushing it up while the bonding nature dropping it down and thus the bands dispersed. In this way, it is very clear that when the conduction and valence bands spread the band gap energy decreases. But in these compounds the CBM is near to a nonbonding hybrid states while VBM have the antibonding states, and hence the CBM will shift by a lesser amount than the VBM upon raising the compression due to

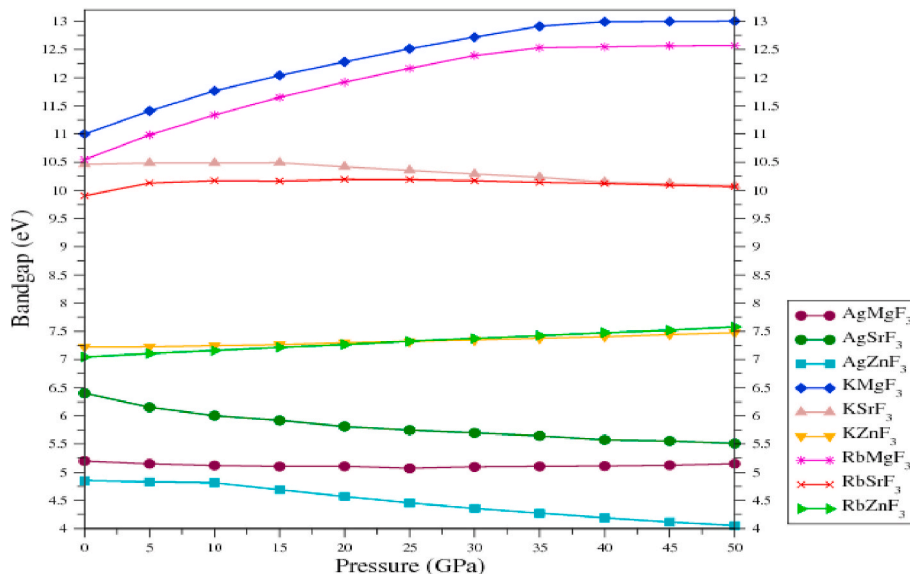


**Fig. 4.** The pressure dependent band gap,  $E_g$  (eV) for  $XYF_3$  ( $X = K, Rb, Ag; Y = Zn, Sr, Mg$ ) under a set of pressure up to 50 GPa.

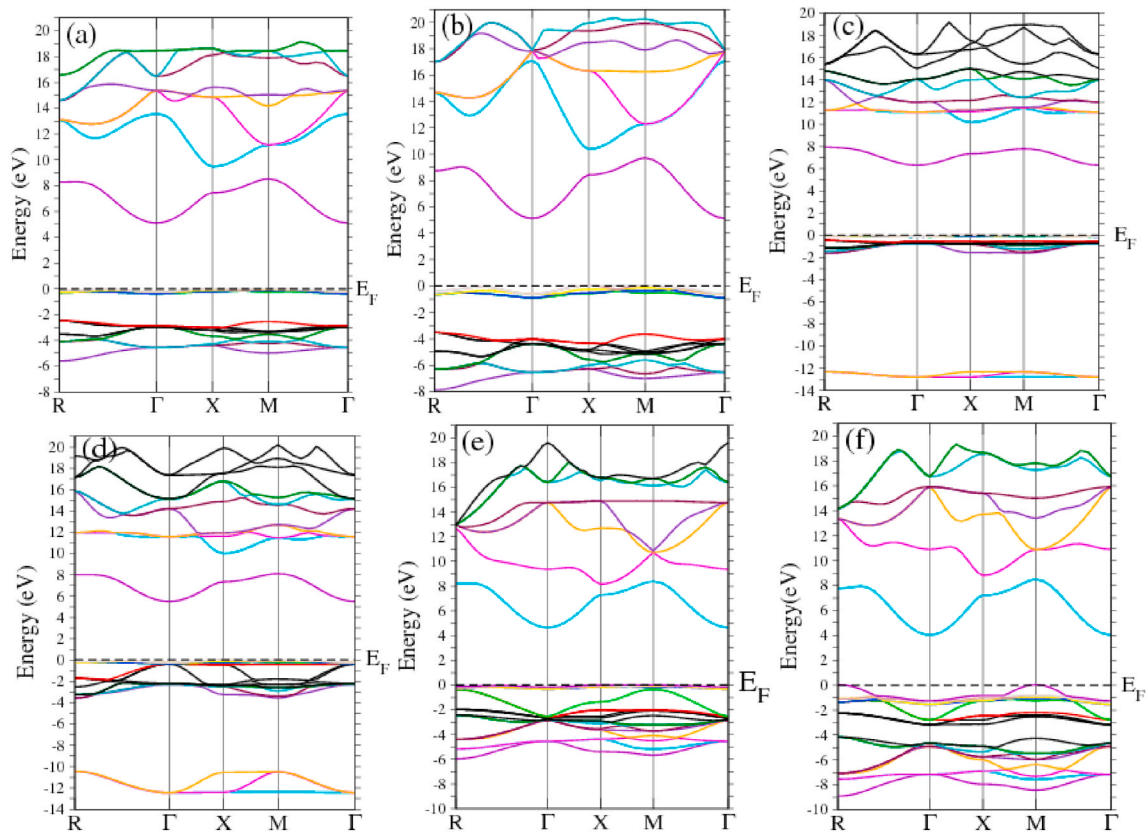


Fig. 5. Band structures of AgMgF<sub>3</sub> (a, b), AgSrF<sub>3</sub> (c, d) and AgZnF<sub>3</sub> (e, f) under 0 GPa (a, c, e) and 50 GPa (b, d, f).

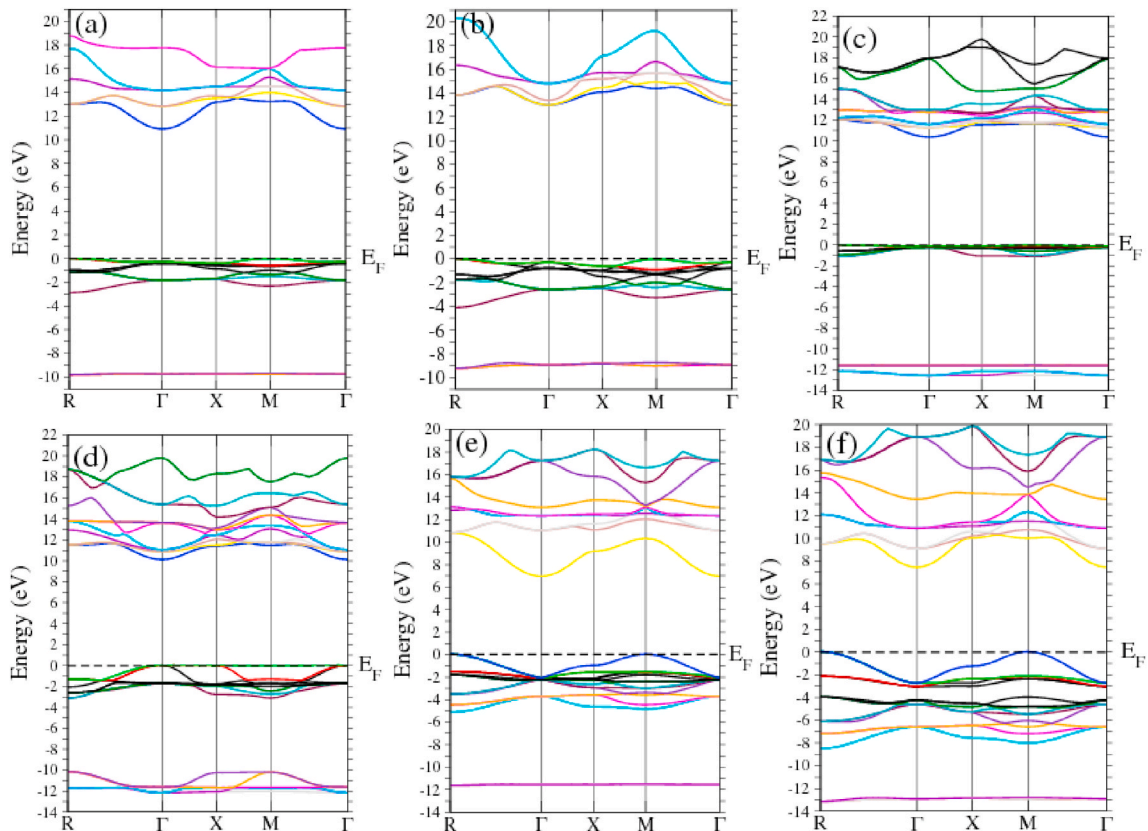


Fig. 6. (a) and (b) are the calculated band structures of KMgF<sub>3</sub> at 0 GPa and 50 GPa, respectively, (b) and (d) are of KSrF<sub>3</sub> at zero and high pressure (50 GPa), and (e) and (f) are of KZnF<sub>3</sub> at zero pressure and 50 GPa respectively.

pressure.

The band gap energy versus pressure diagram shows that the band gap of  $\text{KMgF}_3$ ,  $\text{RbMgF}_3$ ,  $\text{KZnF}_3$ , and  $\text{RbZnF}_3$  compounds increases with increasing the pressure as displayed in Fig. 4. This increase in the band gap can be interpreted on the basis of the covalent [36] and ionic [37] bonding character in these compounds. The study of the electron density plots and the DOS of these compounds reveal that mixed covalent and ionic bonding character exist in the compounds. The band structures of  $\text{KZnF}_3$  (Fig. 6e and f), and  $\text{RbZnF}_3$  (Fig. 7e and f) the energy of the bonding state changes relatively small, being close to the optimized volume, whereas the energy of the antibonding state moves up appreciably with volume reduction due to pressure. The main contribution in the band gap opening to the pressure dependence arises from the covalent energy [36]. With pressure, the covalent nature increase in these compounds which cause greater covalent energy and result in the band gap opening. This effect is predominantly due to nonbonding and antibonding nature of bands closer to the Fermi level, which are specifically sensitized to pressure.

The band structures of  $\text{KMgF}_3$  (Fig. 6a and b) and  $\text{RbMgF}_3$  (Fig. 7a and b) shows that the valence band disperse while the conduction band minimum upshifts with pressure. It is because of the antibonding and bonding nature of the conduction band becomes spread, and because of the antibonding character, the CBM upshifts. The band gap opening can also be explaining from the investigation of electron density plots, which show that a reduction in the interatomic separation with pressure is shown by an increase in localization of density of charge all around the atoms and in the interstitial places. The increased localization with pressure creates deeper potentials, forming unoccupied levels in the conduction band minimum harder to access energetically [37]. From Fig. 4, it is clear that all the compounds have energy bandgap higher than 4 eV under all pressures. So these materials are transparent in the visible region, therefore can be used to make transparent lenses.

In addition, we have performed the spin orbit coupling (SOC) calculations. The energy band structures of the compounds further calculated through the mBJ plus SOC as shown in Fig. S1 (supplementary

material) at the zero and 50 GPa. Further the calculated energy bandgaps are also given in Table S1 (supplementary material). It is observed that SOC does not produce any significant changes in these materials. However, no significant variations in the band structure of the compounds is seen. Mostly the SOC is important for the *d* or *f* block elements with highly correlated nature. However, these compounds are high bandgap materials mostly belong to *p* block. Therefore, as a conclusion no valuable SOC effect take place in these materials.

### 3.2.2. Density of state (DOS)

The study of the total and partial density of states (TDOS and PDOS) is very helpful in understanding the band structure along with the participation of different atomic orbitals. Fig. 8, shows the TDOS and PDOS of  $\text{XYF}_3$  ( $X = \text{K, Rb, Ag; Y} = \text{Zn, Sr, Mg}$ ) compounds at zero pressure (Fig. 8 a, c, e, g, i, k, m, o, and q) and at 50 GPa pressure (Fig. 8 b, d, f, h, j, l, n, p and r) of  $\text{AgMgF}_3$ ,  $\text{AgSrF}_3$ ,  $\text{AgZnF}_3$ ,  $\text{KMgF}_3$ ,  $\text{KSrF}_3$ ,  $\text{KZnF}_3$ ,  $\text{RbMgF}_3$ ,  $\text{RbSrF}_3$ , and  $\text{RbZnF}_3$ , respectively. In this work the DOS are calculated by using TB-mBJ approximation.

The valence band of  $\text{AgMgF}_3$  and  $\text{AgSrF}_3$  are mainly ascribed to  $\text{Ag-4d}$  states with a minor participation of the  $\text{F-2p}$  states (Fig. 8 a, c) while that of  $\text{AgZnF}_3$  the main contributions arises from  $\text{F-2p}$  states with a little participation of  $\text{Ag-4d}$  states and  $\text{Zn-3d}$  states (Fig. 8e). These hybridizations in different orbitals indicate that these compounds have covalent nature. In  $\text{AgMgF}_3$ , the conduction band (CB) is located on the top of the Fermi energy level, which is put together by different states of  $\text{F-3p}$ ,  $\text{Mg-(2s, 2p, 3p)}$  and  $\text{Ag-(5s, 4p)}$  as depicted in the figure. In  $\text{AgSrF}_3$  compound, the conduction band lying on top of the Fermi level in the energy range of 6eV–14eV, which consist of 5s and 4p states of Ag, 3d states of Sr and 3p states of F. Similarly, the conduction band of  $\text{AgZnF}_3$  is composed of 5s and 4d states of Ag, 4s states of Zn and 3p states of F.

The total and partial DOS of  $\text{KMgF}_3$ ,  $\text{KSrF}_3$  and  $\text{KZnF}_3$  at zero pressure are investigated and plotted in Fig. 8 (g), 8 (i) and 8 (k), respectively. The valence band of  $\text{KMgF}_3$  is mainly originated from  $\text{F-2p}$  states and dominated over the  $\text{Sr-4p}$  states. These contribution of orbitals reveal that the nature of bonding in  $\text{KMgF}_3$  and  $\text{KSrF}_3$  is mostly ionic and

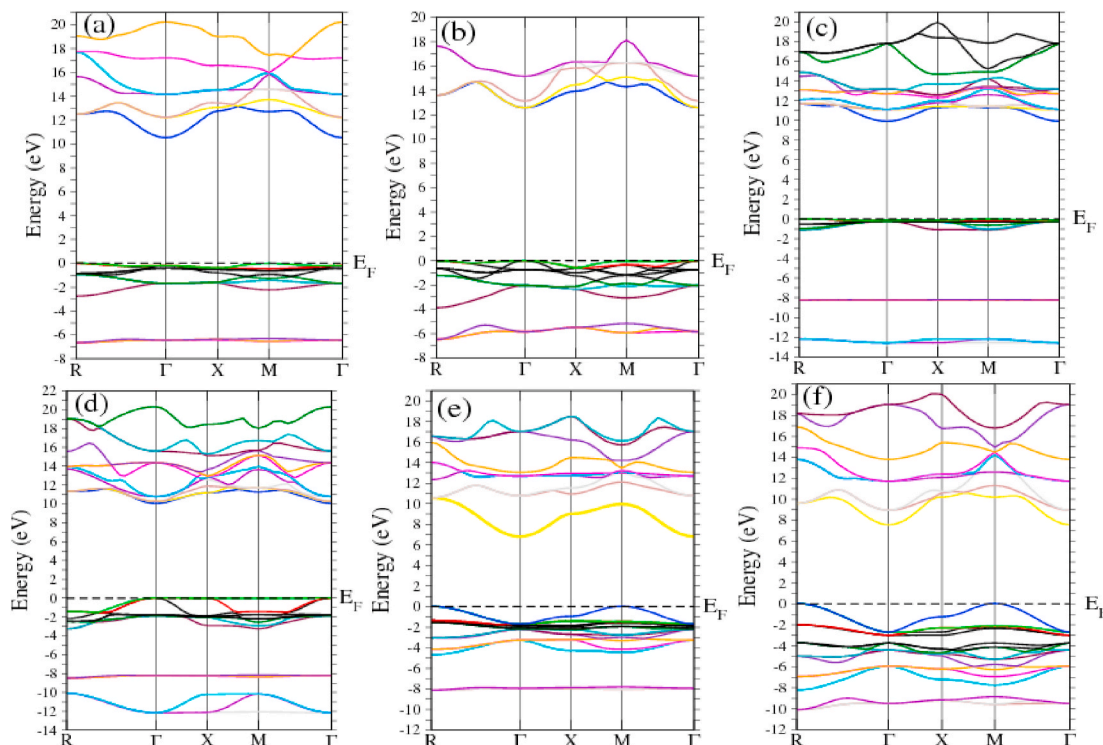
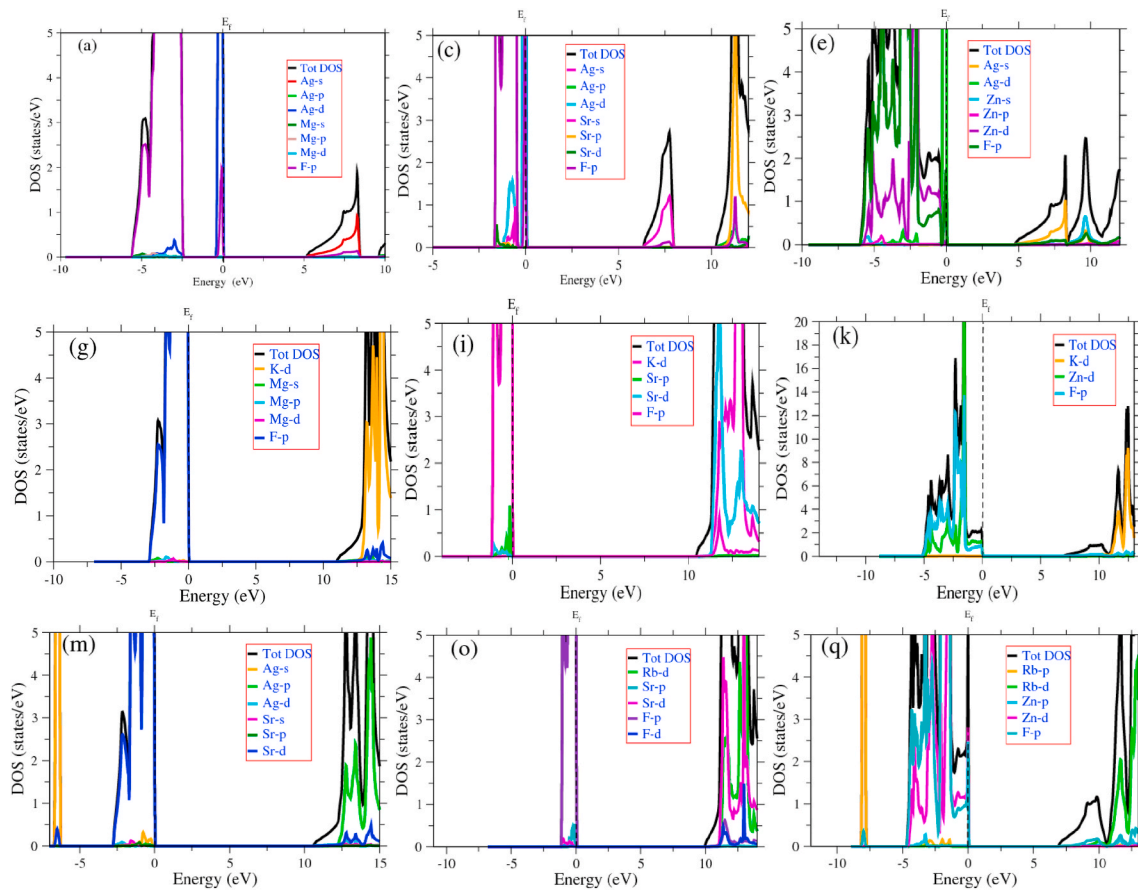


Fig. 7. (a) and (b) are the calculated band structures of  $\text{RbMgF}_3$  at zero and 50 GPa, respectively, (b) and (d) are of  $\text{RbSrF}_3$  at zero and high pressure (50 GPa), and (e) and (f) are of  $\text{RbZnF}_3$  at zero pressure and 50 GPa respectively.



**Fig. 8.** The TDOS and PDOS of AgMgF<sub>3</sub>, AgSrF<sub>3</sub>, AgZnF<sub>3</sub>, KMgF<sub>3</sub>, KSrF<sub>3</sub>, KZnF<sub>3</sub>, RbMgF<sub>3</sub>, RbSrF<sub>3</sub> and RbZnF<sub>3</sub> at zero pressure are presented in (a), (c), (e), (g), (i), (k), (m), (o) and (q) and at 50 GPa pressure in (b), (d), (f), (h), (j), (l), (n), (p) and (r) respectively.

partially covalent. In KZnF<sub>3</sub> compound, the valence band is composed of Mixed F-2p and Zn-3d states. Due to this hybridization of Zn-3d and F-2p states possess the characteristics of strong covalent bond. The conduction band of KMgF<sub>3</sub> is mainly contributed by K-3d states together with small participation of Mg-3s, 3p, 3d and F-3p states while in KSrF<sub>3</sub> the VB (valence band) is populated by mixed K-3d and Sr-3d states. Similarly, the conduction band of KZnF<sub>3</sub> is captured by K-3d states with a minor participation of F-3p states.

The TDOS and PDOS of RbMgF<sub>3</sub>, RbSrF<sub>3</sub> and RbZnF<sub>3</sub> at zero pressure are investigated and plotted in Fig. 8 (m), 8 (o) and 8 (q), respectively. The valence band of RbMgF<sub>3</sub> is mainly originated from F-2p states along with a little participation of Rb-4p and Mg-3d states. These hybridization shows that the bond nature of Rb-F is mainly covalent. In RbSrF<sub>3</sub> compound, the valence band is predominantly because of F-2p states with a minor participation of Sr-4p, 3d and Rb-4p states. In RbZnF<sub>3</sub> compound, the valence band is composed of mixed Zn-3d and F-2p states. Because of the hybridization of Zn-3d and F-2p states possess strong covalent bond characteristics. The conduction band is lying at the top of the Fermi level ( $E_F$ ), Rb-4d mainly contributed to this band with a small contribution from F-3p and Mg-3s, 3p, 3d states in RbMgF<sub>3</sub> compound. In the conduction band of RbSrF<sub>3</sub>, mixed Rb-5p and Sr-4d states occupy this band along with small participation of F-3p and d states. Finally, in the CB of RbZnF<sub>3</sub>, Rb-4d states are mainly contributed to this band along with small contribution from Zn-4s and F-3p states.

The investigation of TDOS as well as PDOS of XYF<sub>3</sub> (X = K, Rb, Ag; Y = Zn, Sr, Mg) compounds under high pressure reveal that the number of states per electron volt (eV) reduces and the bandwidth becomes broader under pressure. The increase in the valence bandwidth under pressure is caused by the strong orbitals hybridization. This

phenomenon reveals that under high pressure these compounds will form covalent bonds in the deeper energy level, and lead to stronger covalent bond strength and hence a reduction in the ionicity.

### 3.2.3. Electron density

The calculated charge density of XYF<sub>3</sub> (X = K, Rb, Ag; Y = Zn, Sr, Mg) compounds in (110) planes, in 2D under zero and 50 GPa are plotted in Fig. 9 to provide visual clarification of the type of bonding among various atoms. The maps of contour plots in view of electron density come up with a vital role in analyzing the chemical bonding nature in crystalline materials [38]. The ionic nature of any compound can be identified by the transfer of charge while the covalent nature can be identified in the charge sharing between the anion and cation. In AgMgF<sub>3</sub>, KMgF<sub>3</sub> and RbMgF<sub>3</sub> compound, the bond between F and Mg is purely ionic, as there is no overlap of the electron density contours (Fig. 9a, (g) and 9(m), respectively). Due to the electronegativity difference between the ions, large amount of charge is moved from the Mg to F. At high pressure (50 GPa), the Mg-F bond is purely ionic in nature as it is claimed from the perfect atomic sphere of Mg, as is visible from the contours of electron density in Fig. 9 (b). Hence, the bond among Mg and F is purely ionic at all the pressure. The electron density distribution among Ag/K/Rb-F is uniform, so the covalent bonding nature exists among the first cation and F. Convincingly, our outcomes approve mixed covalent plus ionic bonding nature in AgMgF<sub>3</sub>, KMgF<sub>3</sub> and RbMgF<sub>3</sub> compound from zero to high pressure (50 GPa).

The electron density contours of AgSrF<sub>3</sub>, KSrF<sub>3</sub> and RbSrF<sub>3</sub> (Fig. 9c, (i) and 9(o), respectively) reveals that the electron density contours overlapping of the Sr and F atoms, and approves Sr-F bond is likely covalent in nature. This covalency in Sr-F is because of the hybridization

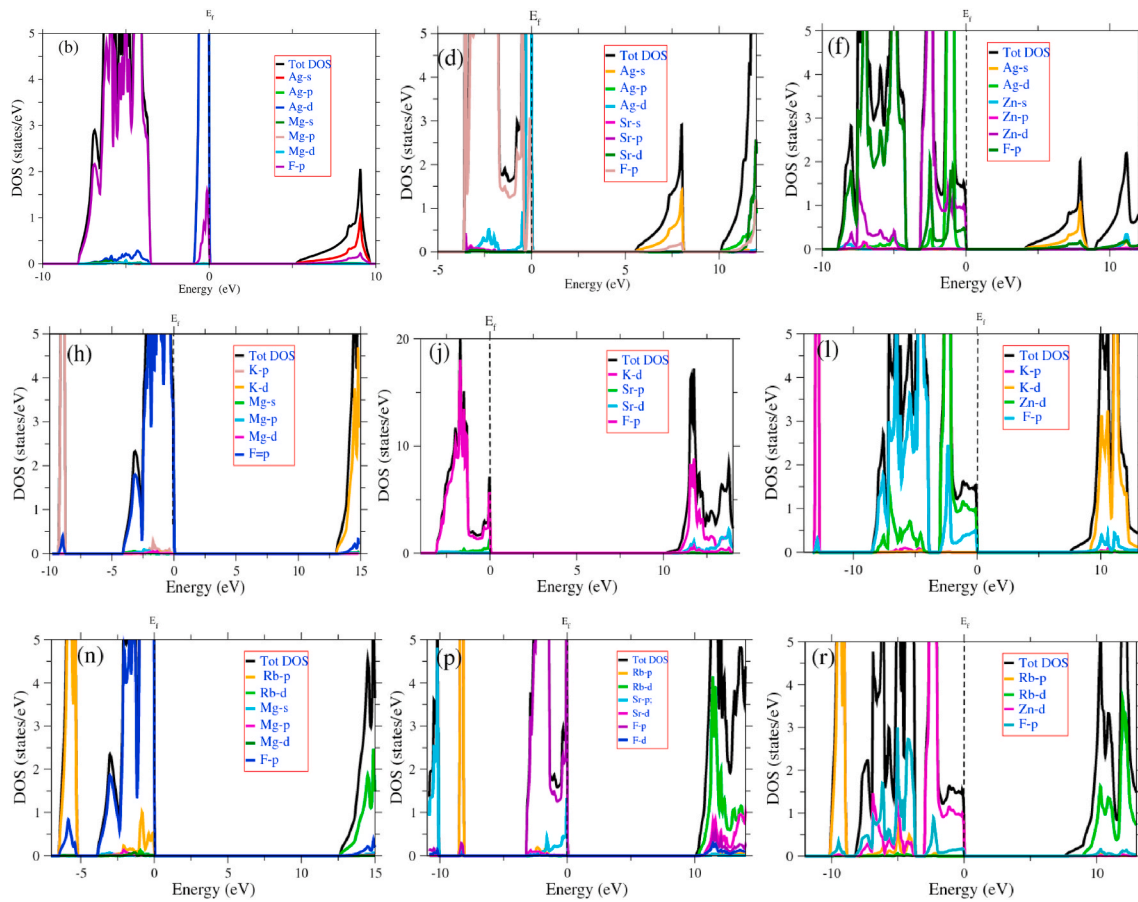


Fig. 8. (continued).

of the Sr-4p and 3d states with F-2p, as can be conformed from the PDOS. Also, the large electronegativity difference between Sr and F, and in return ionic bond between them. So. Mixed (ionic and covalent) bonding nature exist in AgSrF<sub>3</sub> compound. Fig. 9 (d) shows that at high pressure (50 GPa) the overlapping between the electron density contours of Sr and F increases which suggests strong covalent bond at high pressure. Hence, by rising the pressure the covalent bond becomes strong.

The electron density contours of AgZnF<sub>3</sub>, KZnF<sub>3</sub> and RbZnF<sub>3</sub> (Fig. 9e, (k) and 9(q), respectively) reveals that the bond between F and Zn is strongly covalent in nature as can be seen from the electron density contours. This covalent character is due to less difference in electronegativity between F and Zn and pd-hybridization in F-2p and Zn-3d states. Under high pressure the analysis of the electron density contours shows that the overlap increases resulting in covalent interaction by compression.

### 3.3. Optical properties

The knowledge of the interaction of the electromagnetic radiations with matter has unlocked lots of applications of optics in telecommunication, medicine and technology etc. The understanding of the optical properties (linear and non-linear) of the materials is essential to utilize them in different applications. We can understand the concepts of optical properties if we know that how electrons in the condensed matter behave quantum mechanically? Hence, theoretically the optical properties require both convenient and correct formalisms, and the physics of quantum mechanics related to many body systems. DFT is a respectable theoretical tool to study the optical behavior of the solids. In this research, we operated FP-LAPW method to investigate the optical response of XYF<sub>3</sub> (X = K, Rb, Ag; Y = Zn, Sr, Mg) compounds under high

pressure.

When photons of certain energy fall on the matter, it energies the electrons to make the transition from occupied to unoccupied states. From this phenomenon we can gain information about the symmetry of the matter wave associated with electrons and relevant band structure. As the dielectric function  $\epsilon(\omega)$  strongly relies on the frequency, it has a vital impact on the optical properties of the materials. For the interpretation of optical properties, we need to understand the dielectric function of the materials. The complex dielectric function possibly be expressed by the equation given below:

$$\epsilon(\omega) = \epsilon_1(\omega) + i\epsilon_2(\omega) \quad (5)$$

where  $\epsilon(\omega)$  represents the dielectric as a function of frequency  $\omega$ , which describes the electric polarization and absorption of the material. Where  $\epsilon_1(\omega)$  is for real part of dielectric and describes the electric polarization of the material under the external electric field. The real part is determined by the use of Kramers–Kronig relation [39]:

$$\epsilon_1(\omega) = 1 + \frac{2}{\pi} P \int_0^{\infty} \frac{\omega' \epsilon_2(\omega')}{\omega'^2 - \omega^2} d\omega' \quad (6)$$

The frequency dependent imaginary part is denoted by  $\epsilon_2(\omega)$ , which reveals the absorptive behavior of the substance [40]. For cubic symmetry crystals the frequency dependent  $\epsilon_2(\omega)$  is given by [41]:

$$\epsilon_2(\omega) = \frac{8}{2\pi\omega^2} \sum_{nn'} \int_{BZ} |P_{nn'}(k)|^2 \frac{dS_k}{\nabla\omega_{nn'}(k)} \quad (7)$$

where  $|P_{nn'}(k)|$  is for the dipole matrix element between the beginning and last states,  $S_k$  is the constant value of the energy surface and  $\omega_{nn'}(k)$

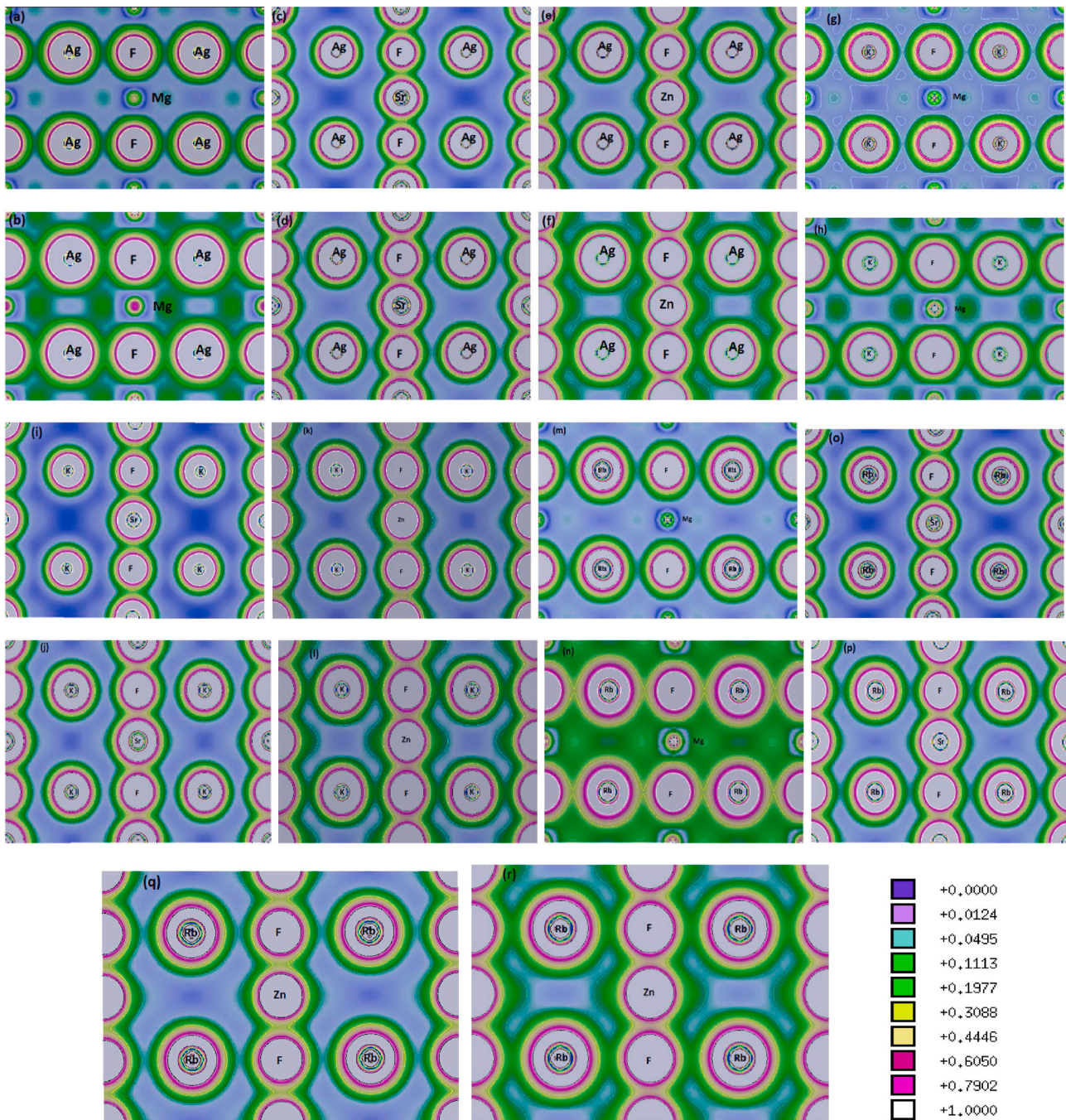


**Fig. 9.** The valence charge density plots ( $e/\text{\AA}^3$ ) in the (110) planes of  $\text{AgMgF}_3$ ,  $\text{AgSrF}_3$ ,  $\text{AgZnF}_3$ ,  $\text{KMgF}_3$ ,  $\text{KSrF}_3$ ,  $\text{KZnF}_3$ ,  $\text{RbMgF}_3$ ,  $\text{RbSrF}_3$  and  $\text{RbZnF}_3$  at zero pressure are presented in (a), (c), (e), (g), (i), (k), (m), (o) and (q) and at 50 GPa pressure in (b), (d), (f), (h), (j), (l), (n), (p) and (r) respectively.

is the difference of energy between two states. The calculated real and imaginary parts of the complex dielectric function can be utilized to find other optical parameters like reflectivity  $R(\omega)$ , refractive index  $n(\omega)$ , optical conductivity and extinction coefficient  $k(\omega)$  [40,42].

The reflectivity ( $R(\omega)$ ), refractive index ( $n(\omega)$ ), optical conductivity ( $\sigma(\omega)$ ) and absorption coefficient ( $\alpha(\omega)$ ) of  $\text{XYF}_3$  ( $X = \text{K, Rb, Ag}$ ;  $Y = \text{Zn, Sr, Mg}$ ) are calculated in the pressure ranging 0–50 GPa with the energy of photon ranging from 0 to 40 eV. From Fig. 3, we can see that peaks of refractive index of all these compounds shift towards the higher energies with rising the pressure, which meaning undergo a blue shift.

### 3.3.1. Refractive index

Fig. 10 depicts the spectrum for refractive index versus energy of  $\text{KMgF}_3$ ,  $\text{RbMgF}_3$ ,  $\text{KZnF}_3$  and  $\text{RbZnF}_3$  compounds under high pressure ranging from 0 to 50 GPa. It is readily apparent from the figure that the static refractive index  $n_0$  increases from 1.4 to 1.7, 1.3 to 1.9, 1.2 to 1.8 and 1.5 to 1.9 for  $\text{KMgF}_3$ ,  $\text{RbMgF}_3$ ,  $\text{KZnF}_3$  and  $\text{RbZnF}_3$  respectively under the rise of pressure in the range 0–50 GPa. This increase in the static refractive index is because of the fact that the reduction in the volume of the substance under high pressure increase the number of electronic oscillators per unit volume and hence increase the refractive index. Which is in accordance to the photo-elasticity theory (Mueller 1935) [43], according to this theory the variation in the refractive index under

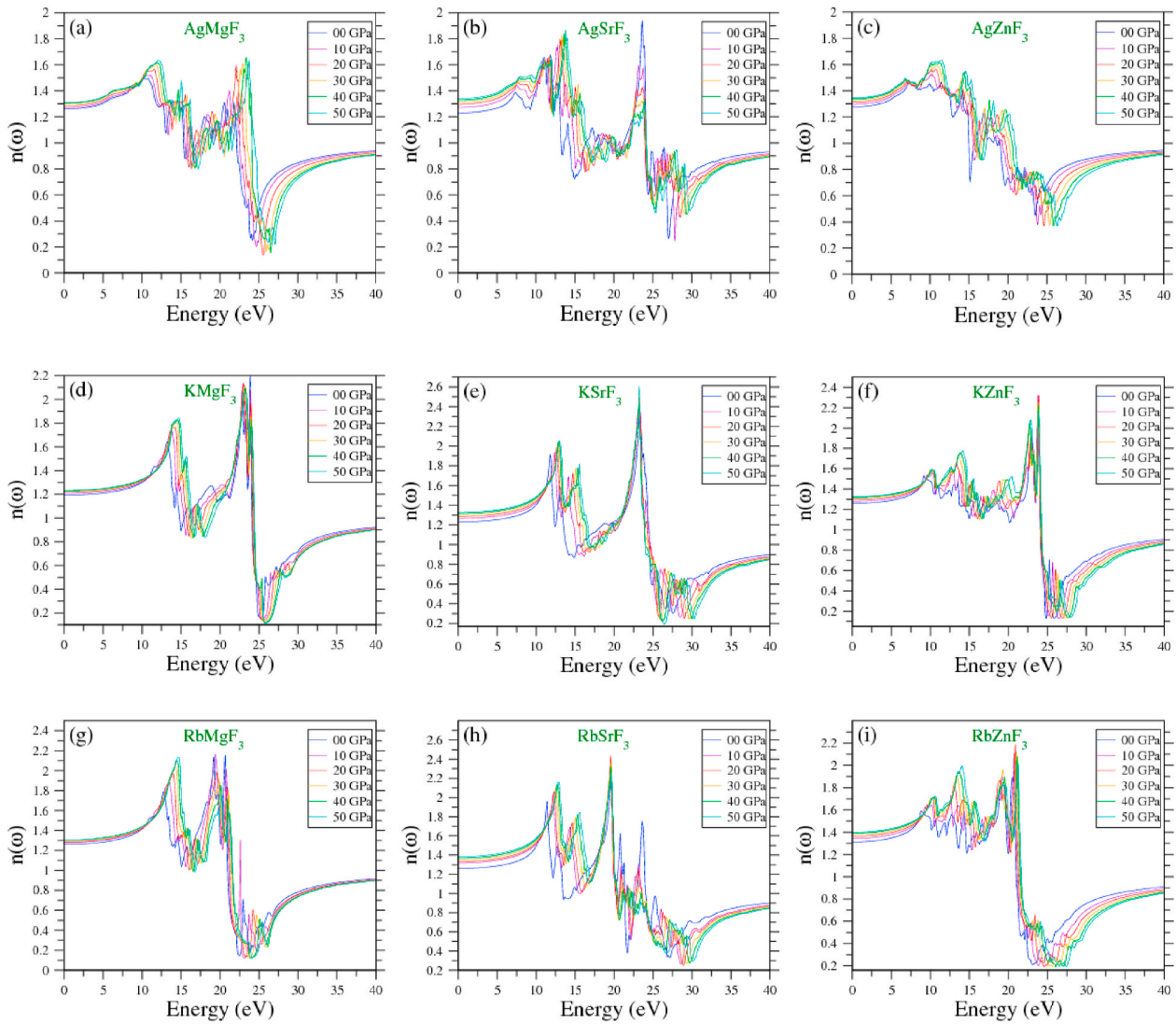


**Fig. 10.** The refractive index as a function of photon energy of  $XYF_3$  ( $X = K, Rb, Ag; Y = Zn, Sr, Mg$ ) under high pressure (0–50 GPa).

the influence of pressure is because of the alterations in the quantity of oscillators in a unit volume (in other words, the change in the density of the material), and variations in the polarizability of ions or also in atoms mainly because of the size of the unit cell. The direct effect of pressure on the material is the increase of density, and hence result in increase in the refractive index of the material.

We can also see that the peak in the refractive index spectrum shifts toward higher energy (blue shift) as the pressure increases. The reason behind this phenomenon goes on as by increasing the pressure, the band gap of these compounds become wider, now electrons need more energy to make transition from VB to CB increases, due to this, the peak position is blue shifted. Consequently, it is attributed to the fact that beyond a certain value of energy (band gap  $E_g$ ), the transparent nature of material will no longer be maintained, and high energy photons are ready to be absorbed. At certain value of energy, the refractive index exhibit values lower than unity. Refractive index with value less than unity illustrates that phase velocity possessed by incident radiation inside the material turn out to be greater than speed of light.

Fig. 10 also shows the refractive index as a function of photon energy of  $KSrF_3$ ,  $AgSrF_3$  and  $AgZnF_3$  compounds under pressure (0–50 GPa). The refractive index spectrum of these compounds under pressure behave in the same way as shown in Fig. 10. However, there is contraction in the band gap with the rise in the pressure, therefore, the blue shift in the peaks of the refractive indices is due to the broadening

of the band structure under external pressure.

The refractive index spectrum of  $RbSrF_3$  and  $AgMgF_3$  are also shown in Fig. 10. Under external pressure, the static refractive indices of these compounds increase and the peaks exist in the spectrum shifts towards the higher energies (blue shift).

### 3.3.2. Reflectivity

The mathematical expression for reflectivity  $R(\omega)$  in terms of  $\epsilon_1(\omega)$  and  $\epsilon_2(\omega)$  is given below [60–62]:

$$n(\omega) = \frac{1}{\sqrt{2}} \left[ \left\{ \epsilon_1(\omega)^2 + \epsilon_2(\omega)^2 \right\}^{\frac{1}{2}} + \epsilon_1(\omega) \right]^{\frac{1}{2}} \quad (8)$$

$$k(\omega) = \frac{1}{\sqrt{2}} \left[ \left\{ \epsilon_1(\omega)^2 + \epsilon_2(\omega)^2 \right\}^{\frac{1}{2}} - \epsilon_1(\omega) \right]^{\frac{1}{2}} \quad (9)$$

$$R = \frac{(n-1)^2 + k^2}{(n+1)^2 + k^2} \quad (10)$$

From above equation it is clear that the reflectivity depends on the refractive index  $n(\omega)$  and extinction coefficient  $k(\omega)$  of the material. In other words, the reflectivity depends on the speed of electromagnetic

radiation inside the material, and also depends on the damping or the decay of the incident electric field amplitude.

The reflectivity spectra under high pressure of  $XYF_3$  ( $X = K, Rb, Ag$ ;  $Y = Zn, Sr, Mg$ ) compounds are depicted in Fig. 11. In the  $KMgF_3$ ,  $RbMgF_3$ ,  $KZnF_3$  and  $RbZnF_3$  compounds the reflectivity peaks shift towards the higher energies (blue shift) as we increase the pressure. It is because of the rise in the band gap energy and the broadening of the valence and conduction bands with increase in pressure, which increase the energy of the interband transition. The reflectivity versus photon energy plots of  $KSrF_3$ ,  $AgZnF_3$ ,  $AgMgF_3$ ,  $AgSrF_3$  and  $RbSrF_3$  are also shown in Fig. 11. We can clearly see the blue shift in the reflectivity spectra of these compounds because of the broadening of the conduction and valence band.

### 3.3.3. Optical conductivity

Electrical conductivity of a material in the presence of electromagnetic radiations is termed as optical conductivity. The mathematical equation for optical conductivity as a function of frequency is given by:

$$\sigma(\omega) = \frac{2W_{ev}9\hbar\omega}{\rightarrow E_0} \quad (11)$$

where  $W_{ev}$  represents the transition probability per second (unit time).

Fig. 12 shows the optical conductivity spectrum versus photons energy of  $XYF_3$  ( $X = K, Rb, Ag$ ;  $Y = Zn, Sr, Mg$ ), under high pressure ranging

0–50 GPa. Every peak in the optical conductivity spectrum is due to the interband transitions of electrons. The optical conductivity spectrum of these compounds reveals a blue shift, and the height of the small peaks increase with pressure due to band dispersion upon increasing the orbital overlap with compression. In other words, the optical conductivity is proportional to the density of free electrons and holes. Hence, the optical conductivity increases due to the production of free carriers, when electrons absorb the photons and make interband transitions. Large number of carrier concentration is responsible for high optical conductivity. Hence, the increase in the optical conductivity because of the increase in the joint density of states. Blue shift of the conductivity peaks is more visible for those compounds whose bandgap increases with the pressure. However, all the compounds show blue shift due to the increases in the width of valence band. It can be seen from Fig. 12 that the height of the maximum peak decrease with pressure for  $KMgF_3$ ,  $KZnF_3$ ,  $RbMgF_3$  and  $RbZnF_3$  because of increase in the bandgap energy.

### 3.3.4. Absorption coefficient

It is highly important to study the absorption ability of a material for its possible application in optical devices. The absorption coefficient  $\alpha(\omega)$ , which illustrate the attenuation of the electromagnetic radiations in the material shown in Fig. 13 as a function of energy of  $XYF_3$  ( $X = K, Rb, Ag$ ;  $Y = Zn, Sr, Mg$ ) compounds under high pressure. The investigation of these absorption spectra reveals that these absorption spectra is blue

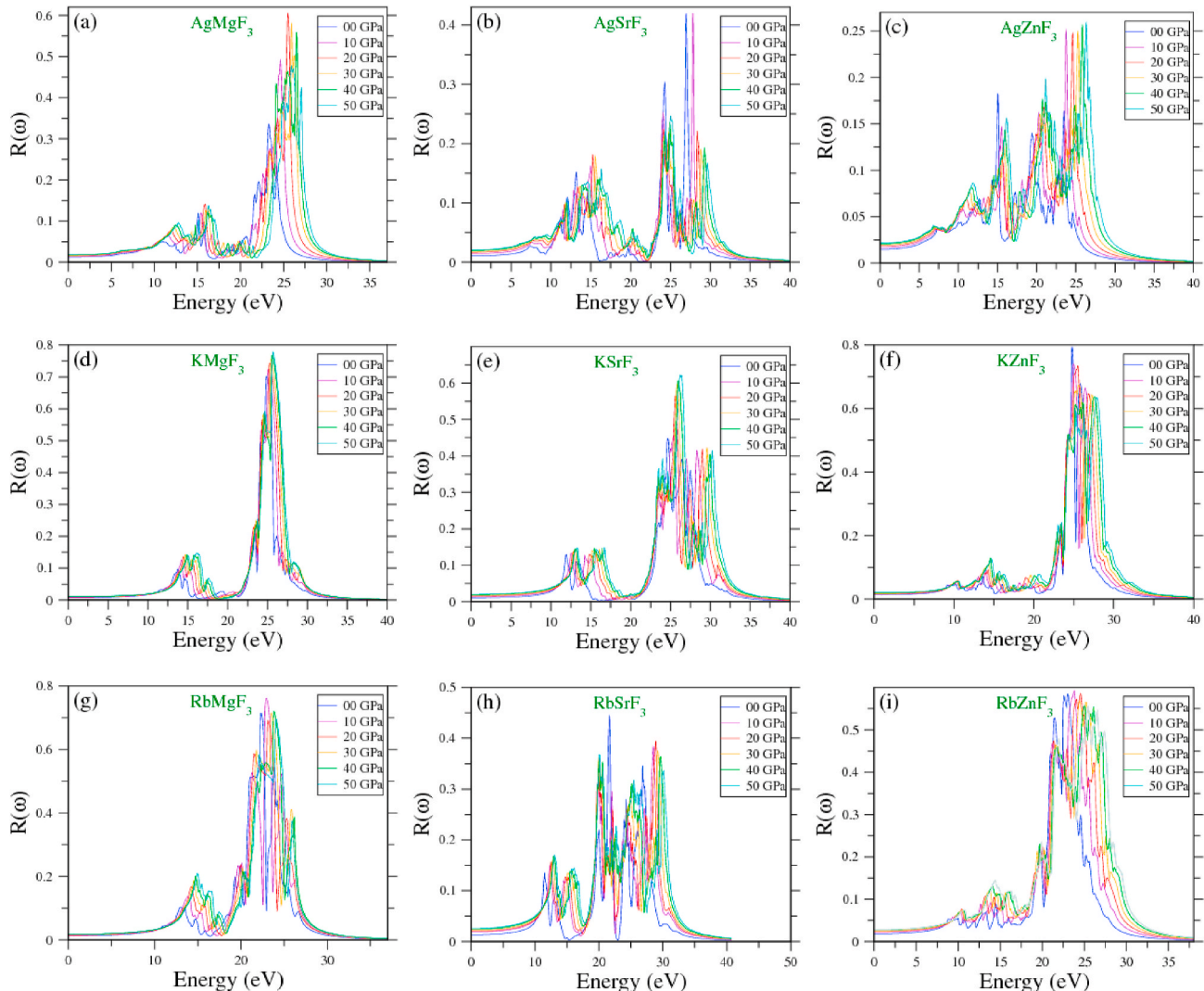
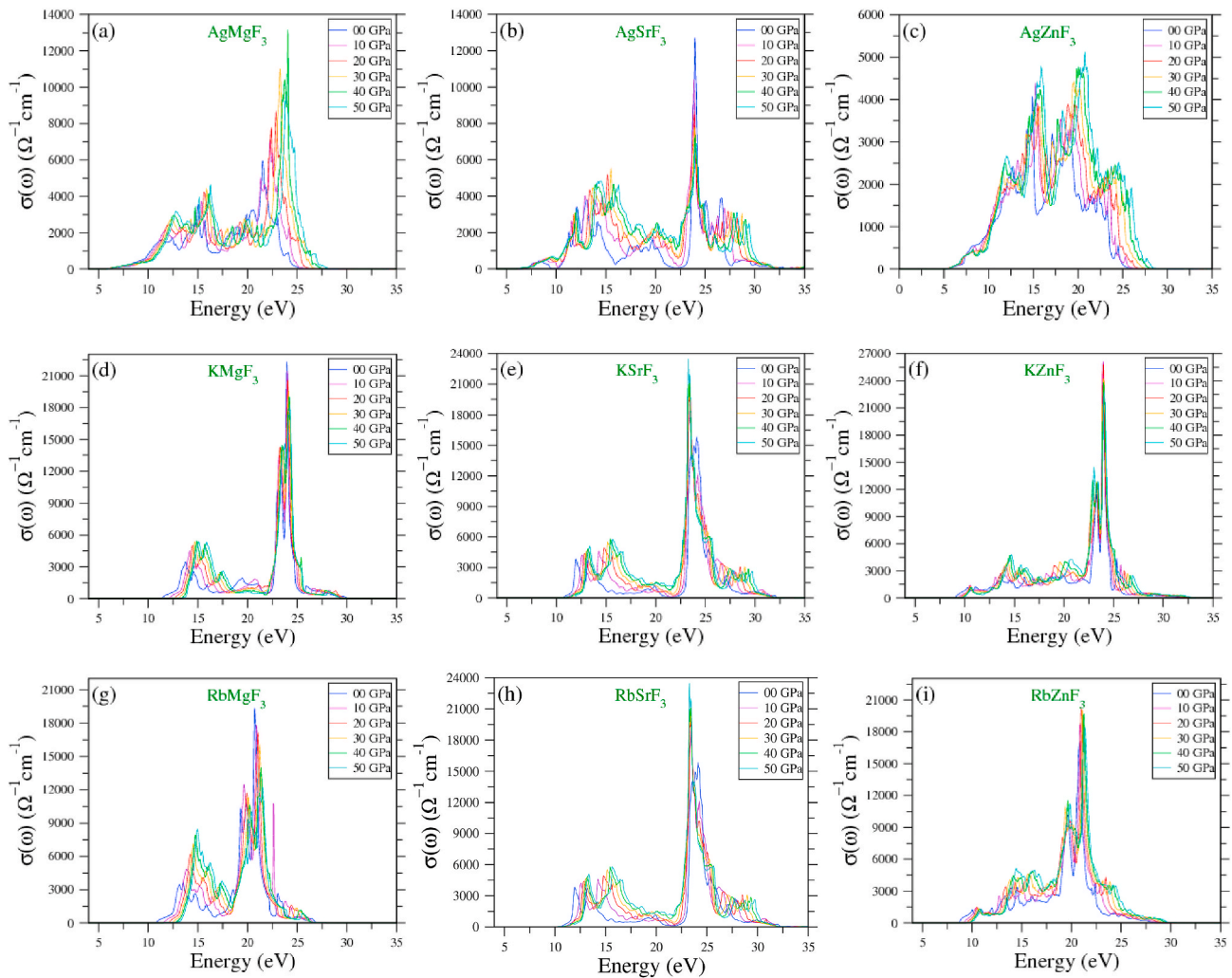


Fig. 11. The reflectivity as a function of photon energy of  $XYF_3$  ( $X = K, Rb, Ag$ ;  $Y = Zn, Sr, Mg$ ) under high pressure.



**Fig. 12.** The optical conductivity as a function of photon energy of  $XYF_3$  ( $X = K, Rb, Ag; Y = Zn, Sr, Mg$ ) under high pressure.

shifted (moved towards high energy). The blue shift in the absorption spectrum of  $RbZnF_3$ ,  $KZnF_3$ ,  $KMgF_3$ , and  $RbMgF_3$  compounds is because of two factors, firstly as the pressure increase the band gap of these compounds increases, and secondly, with pressure the bands of these compound spreads and become wider. The increase in the band gap energy and the spreading of bands with pressure allow more energetic photons to make interband transitions from the valence band (VC) to conduction (CB). While the blue shift in the other compounds is only because of the spreading of bands with pressure. Overall the absorption peaks at lower energy increases with the increases in pressure and therefore can be very effective for enhancing device efficiency. These compounds have energy bandgaps higher than the visible region therefore can be effectively used for the high frequency devices working the ultraviolet region e.g. radiation detectors, scintillators, transparent lenses.

#### 4. Conclusions

Important fluoroperovskites  $XYF_3$  ( $X = K, Rb, Ag; Y = Zn, Sr, Mg$ ) compounds have been investigated in a wide pressure range (0–50 GPa). It is observed that the unit cell volume and lattice constant decreases with the increase of pressure. While this decrease is rapid at lower pressure compared to higher pressure. Electronically, these compounds are all indirect wide band gap insulators, the band gap values are compared with available theoretical as well as experimental works. Under the impact of high pressure (0–50 Gpa) the band gap of  $AgMgF_3$ ,

$KMgF_3$ ,  $KZnF_3$ ,  $RbMgF_3$  and  $RbZnF_3$  compounds increases with pressure. This is because of the inverse relations with the lattice constant. The band of gap of  $AgZnF_3$  and  $KSrF_3$  first increases from zero to 10 GPa and 5 GPa respectively and then decreases smoothly with pressure up to 50 GPa. The band gap of  $RbSrF_3$  and  $KSrF_3$  change form indirect to direct at a pressure of 5 GPa. The DOS and electron density are also investigated at zero and 50 GPa pressure. It is determined that covalent bond exist in  $Ag-F$ ,  $Zn-F$ . The bonding nature of  $Mg-F$  is purely ionic while the bond between  $Sr$  and  $F$  is partially covalent and ionic.  $K-F$  and  $Sr-F$  bonds are partially ionic and partially covalent in nature. Under high pressure the covalent interactions increase which shows that there will be higher covalent bonding nature under high pressure. These compounds show maximum reflectivity for photons having energy in between 20 eV and 30 eV, which is the high ultraviolet region of spectrum. Under high pressure the reflectivity peaks shift towards higher energy with the increase in pressure. At zero frequency limit, the refractive index of these compounds increases under pressure, this increase in the refractive index is purely pressure dependent. Also, we observed that the refractive index peaks shift towards the right energy level and their height also increase with pressure while their trough becomes deeper and also shift towards right energy level. Similarly, the optical conductivity and absorption coefficient spectra structures shift towards the higher energies. The absorption enhances with the increase of pressure. These materials can be used for the high frequency optoelectronic devices.

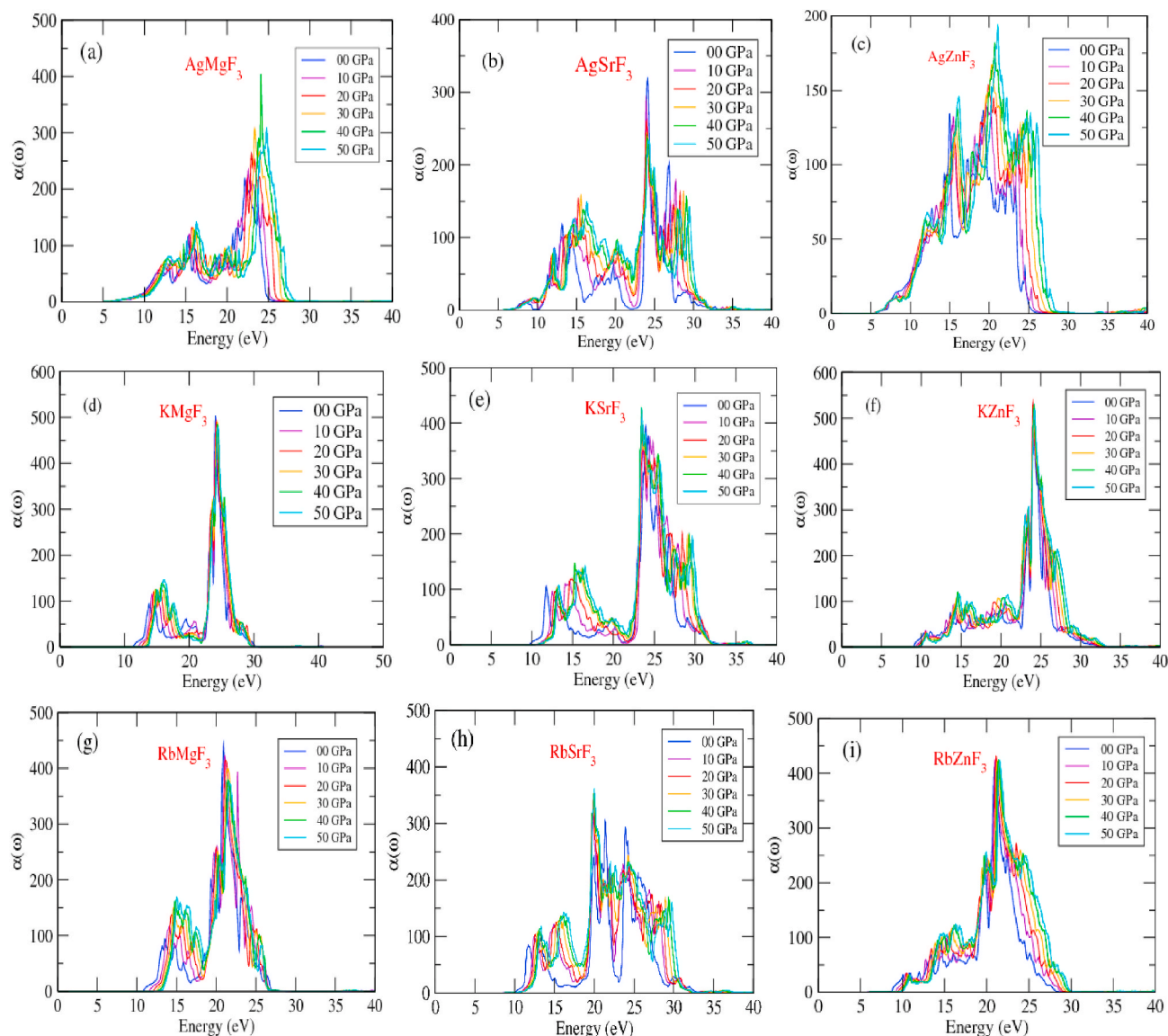


Fig. 13. The absorption coefficient as a function of photon energy of  $XYF_3$  ( $X = K, Rb, Ag; Y = Zn, Sr, Mg$ ) under high pressure.

### Declaration of competing interest

The authors declare that they have no known competing financial interests or personal relationships that could have appeared to influence the work reported in this paper.

### Acknowledgements

For the author (A. Laref) this research project was supported by a grant from the “Research Center of Female Scientific and Medical Colleges”, Deanship of Scientific Research, King Saud University.

### Appendix A. Supplementary data

Supplementary data to this article can be found online at <https://doi.org/10.1016/j.optmat.2020.110325>.

### References

- [1] J.W. Anthony, R.A. Bideaux, K.W. Bladh, M.C. Nichols, *Handbook of Mineralogy*, Mineralogical Society of America, Chantilly, VA, USA, 2011.
- [2] F. Zhang, Y. Mao, T.J. Park, S.S. Wong, Green synthesis and property characterization of single-crystalline perovskite fluoride nanorods, *Adv. Funct. Mater.* 18 (1) (2008) 103–112.
- [3] A.V. Gektin, I.M. Krasovitskaya, N.V. Shiran, High-temperature thermoluminescence of  $KMgF_3$ -based crystals, *J. Lumin.* 72 (1997) 664–666.
- [4] M. Eibschütz, H.J. Guggenheim, Antiferromagnetic-piezoelectric crystals:  $BaMe_4$  ( $M = Mn, Fe, Co$  and  $Ni$ ), *Solid State Commun.* 6 (10) (1968) 737–739.
- [5] P. Berastegui, S. Hull, S.G. Eriksson, A low-temperature structural phase transition in  $CsPbF_3$ , *J. Phys. Condens. Matter* 13 (22) (2001) 5077.
- [6] R.R. Daniels, G. Margaritondo, R.A. Heaton, C.C. Lin, Experimental study of the electronic structure of  $KMgF_3$ , *Phys. Rev. B* 27 (6) (1983) 3878.
- [7] J. Julliard, J. Nouet, Analyse radiocristallographique de la distorsion magnétostrictive dans les antiferromagnétiques  $KCoF_3$ ,  $RbCoF_3$  et  $TlCoF_3$ , *Rev. Phys. Appl.* 10 (5) (1975) 325–329.
- [8] R. Hua, B. Lei, D. Xie, C. Shi, Synthesis of the complex fluoride  $LiBaF_3$  and optical spectroscopy properties of  $LiBaF_3$ : M ( $M = Eu, Ce$ ) through a solvothermal process, *J. Solid State Chem.* 175 (2) (2003) 284–288.
- [9] M. Sahnoun, M. Zbiri, C. Daul, R. Khenata, H. Baltache, M. Driz, Full potential calculation of structural, electronic and optical properties of  $KMgF_3$ , *Mater. Chem. Phys.* 91 (1) (2005) 185–191.
- [10] G. Hörsch, H.J. Paus, A new color center laser on the basis of lead-doped  $KMgF_3$ , *Optic Commun.* 60 (1–2) (1986) 69–73.
- [11] T. Nishimatsu, N. Terakubo, H. Mizuseki, Y. Kawazoe, D.A. Pawlak, K. Shimamura, T. Fukuda, Band structures of perovskite-like fluorides for vacuum-ultraviolet-transparent lens materials, *Jpn. J. Appl. Phys.* 41 (4A) (2002) L365.
- [12] C. Dotzler, G.V.M. Williams, A. Edgar, Radiation-induced optically and thermally stimulated luminescence in  $RbCdF_3$  and  $RbMgF_3$ , *Curr. Appl. Phys.* 8 (3–4) (2008) 447–450.

- [13] A.A. Mubarak, A.A. Mousa, The electronic and optical properties of the fluoroperovskite  $\text{BaXF}_3$  ( $X = \text{Li, Na, K, and Rb}$ ) compounds, *Comput. Mater. Sci.* 59 (2012) 6–13.
- [14] Y. Wang, L. Bai, T. Wen, L. Yang, H. Gou, Y. Xiao, P. Chow, M. Pravica, W. Yang, Y. Zhao, Giant pressure-driven lattice collapse coupled with intermetallic bonding and spin-state transition in manganese chalcogenides, *Angew. Chem. Int. Ed.* 55 (35) (2016) 10506–10509.
- [15] G. Xiao, X. Yang, X. Zhang, K. Wang, X. Huang, Z. Ding, Y. Ma, G. Zou, B. Zou, A protocol to fabricate nanostructured new phase: B31-type  $\text{MnS}$  synthesized under high pressure, *J. Am. Chem. Soc.* 137 (32) (2015) 10297–10303.
- [16] G. Xiao, K. Wang, L. Zhu, X. Tan, Y. Qiao, K. Yang, Y. Ma, B. Liu, W. Zheng, B. Zou, Pressure-Induced reversible phase transformation in nanostructured  $\text{Bi}_2\text{Te}_3$  with reduced transition pressure, *J. Phys. Chem. C* 119 (7) (2015) 3843–3848.
- [17] G. Xiao, C. Zhu, Y. Ma, B. Liu, G. Zou, B. Zou, Unexpected room-temperature ferromagnetism in nanostructured  $\text{Bi}_2\text{Te}_3$ , *Angew. Chem. Int. Ed.* 126 (3) (2014) 748–752.
- [18] S.T. John, Crystallography of selected high pressure elemental solids, *Z. für Kristallogr. - Cryst. Mater.* 220 (5/6) (2005) 521–530.
- [19] B. Ghebouli, M.A. Ghebouli, M. Fatmi, A. Bouhemadou, First-principles study of the structural, elastic, electronic, optical and thermodynamic properties of the cubic perovskite  $\text{CsCdCl}_3$  under high pressure, *Solid State Commun.* 150 (39–40) (2010) 1896–1901.
- [20] T. Seddik, R. Khenata, O. Merabih, A. Bouhemadou, S. Bin-Omran, D. Rached, Elastic, electronic and thermodynamic properties of fluoro-perovskite  $\text{KZnF}_3$  via first-principles calculations, *Appl. Phys. A* 106 (3) (2012) 645–653.
- [21] S. Cui, W. Feng, H. Hu, Z. Feng, Y. Wang, High-pressure structural, electronic and optical properties of  $\text{KMgF}_3$ : a first-principles study, *J. Alloys Compd.* 484 (1–2) (2009) 597–600.
- [22] B. Sahli, H. Bouafia, B. Abidri, A. Bouaza, A. Akriche, S. Hiadsi, A. Abdellouli, Study of hydrostatic pressure effect on structural, mechanical, electronic and optical properties of  $\text{KMgF}_3$ ,  $\text{K}_{0.5}\text{Na}_{0.5}\text{MgF}_3$  and  $\text{NaMgF}_3$  cubic fluoro-perovskites via ab-initio calculations, *Int. J. Mod. Phys. B* 30 (32) (2016) 1650230.
- [23] G. Vaitheeswaran, V. Kanchana, R.S. Kumar, A. Cornelius, M. Nicol, A. Svane, A. Delin, B. Johansson, High-pressure structural, elastic, and electronic properties of the scintillator host material  $\text{KMgF}_3$ , *Phys. Rev. B* 76 (1) (2007), 014107.
- [24] A.H. Larbi, F. Bouzid, M. Hadjab, A. Naas, S. Hiadsi, The variation of the gap with hydrostatic pressure of the fluoroperovskite  $\text{RbZnF}_3$  compound, in: *The 7th African Conference on Non Destructive Testing, ACNDT*, 2016.
- [25] F. Aguado, F. Rodríguez, S. Hirai, J.N. Walsh, A. Lennie, S.A. Redfern, High-pressure behaviour of  $\text{KMgF}_3$  perovskites, *High Pres. Res.* 28 (4) (2008) 539–544.
- [26] A. Meziani, D. Heciri, H. Belkhir, Structural, electronic, elastic and optical properties of fluoro-perovskite  $\text{KZnF}_3$ , *Phys. B Condens. Matter* 406 (19) (2011) 3646–3652.
- [27] F.D. Murnaghan, The compressibility of media under extreme pressures, *Proc. Natl. Acad. Sci. U.S.A.* 30 (9) (1944) 244.
- [28] H. Bouafia, S. Hiadsi, B. Abidri, A. Akriche, L. Ghalouci, B. Sahli, Structural, elastic, electronic and thermodynamic properties of  $\text{KTaO}_3$  and  $\text{NaTaO}_3$ : ab-initio investigations, *Comput. Mater. Sci.* 75 (2013) 1–8.
- [29] G.I. Csonka, J.P. Perdew, A. Ruzsinszky, P.H. Phillipsen, S. Lebègue, J. Paier, O. A. Vydrov, J.G. Ángyán, Assessing the performance of recent density functionals for bulk solids, *Phys. Rev. B* 79 (15) (2009) 155107.
- [30] B. Sahli, H. Bouafia, B. Abidri, A. Abdellouli, S. Hiadsi, A. Akriche, N. Benkhetou, D. Rached, First-principles prediction of structural, elastic, electronic and thermodynamic properties of the cubic  $\text{SrUO}_3$ -Perovskite, *J. Alloys Compd.* 635 (2015) 163–172.
- [31] F.D. Murnaghan, *Proc. Natl. Acad. Sci. U.S.A.* 30 (1944) 244, 30 (1944) 244.
- [32] F.E.H. Hassan, M. Zoeter, A. Hijazi, Structural and electronic properties of bcc selenium under high pressure, *Fizika* 14 (3) (2005) 245–254.
- [33] R. Mousa, A. Abdiche, B. Abbar, M. Guemou, R. Riane, G. Murtaza, S.B. Omran, R. Khenata, F. Soyalp, Ab initio investigation of the structural, electronic and optical properties of cubic  $\text{GaAs}_{1-x}\text{Px}$  ternary alloys under hydrostatic pressure, *J. Electron. Mater.* 44 (12) (2015) 4684–4699.
- [34] Y. Al-Douri, A.H. Reshak, Calculated optical properties of  $\text{GaX}$  ( $X = \text{P, As, Sb}$ ) under hydrostatic pressure, *Appl. Phys. A* 104 (4) (2011) 1159.
- [35] R.K. Willardson, E.R. Weber, W. Paul, T. Suski, *High Pressure Semiconductor Physics I*, Academic Press, 1998.
- [36] T. Suski, W. Paul, *High Pressure Semiconductor Physics I*, Academic Press, 1998.
- [37] J.S. Kearney, M. Grauzinyte, D. Smith, D. Sneed, C. Childs, J. Hinton, C. Park, J. S. Smith, E. Kim, S.D. Fitch, Pressure-tunable visible-range band gap in the ionic spinel tin nitride, *Angew. Chem. Int. Ed.* 57 (36) (2018) 11623–11628.
- [38] C. Kittel, *Introduction to Solid State Physics*, John Wiley & Sons, Inc., New York, 2005.
- [39] 龍. 尾中, F. Wooten, *Optical Properties of Solids*, 28, Academic Press, New York and London, 1972, pp. 803–804, 1973.
- [40] G. Murtaza, I. Ahmad, B. Amin, A. Afaq, M. Maqbool, J. Maqssod, I. Khan, M. Zahid, Investigation of structural and optoelectronic properties of  $\text{BaThO}_3$ , *Opt. Mater.* 33 (3) (2011) 553–557.
- [41] M.A. Khan, A. Kashyap, A.K. Solanki, T. Nautiyal, S. Auluck, Interband optical properties of  $\text{Ni}_3\text{Al}$ , *Phys. Rev. B* 48 (23) (1993) 16974.
- [42] G. Murtaza, I. Ahmad, B. Amin, A. Afaq, F. Ghafoor, A. Benamrani, Linear and nonlinear optical response of  $\text{Mg}_x\text{Zn}_{1-x}\text{O}$ : a density functional study, *Phys. B Condens. Matter* 406 (13) (2011) 2632–2636.
- [43] H. Mueller, Theory of the photoelastic effect of cubic crystals, *Phys. Rev.* 47 (12) (1935) 947.
- [44] G.A. Geguzina, V.P. Sakhnenko, Correlation between the lattice parameters of crystals with perovskite structure, *Crystallogr. Rep.* 49 (1) (2004) 15–19.
- [45] R. Roy, O. Muller, *The Major Ternary Structural Families*, Springer-Verlag, Berlin, 1974.
- [46] G. Murtaza, G. Sadique, H.R. Aliabad, M.N. Khalid, S. Naeem, A. Afaq, B. Amin, I. Ahmad, First principle study of cubic perovskites:  $\text{AgTF}_3$  ( $T = \text{Mg, Zn}$ ), *Phys. B Condens. Matter* 406 (24) (2011) 4584–4589.
- [47] A.S. Verma, A. Kumar, S.R. Bhardwaj, Correlation between ionic charge and the lattice constant of cubic perovskite solids, *Phys. Status Solidi* 245 (8) (2008) 1520–1526.
- [48] R.L. Moreira, A. Dias, Comment on Prediction of lattice constant in cubic perovskites, *J. Phys. Chem. Solid.* 68 (8) (2007) 1617–1622.
- [49] L.Q. Jiang, J.K. Guo, H.B. Liu, M. Zhu, X. Zhou, P. Wu, C. Li, Prediction of lattice constant in cubic perovskites, *J. Phys. Chem. Solid.* 67 (7) (2006) 1531–1536.
- [50] S. Hiadsi, H. Bouafia, B. Sahli, B. Abidri, A. Bouaza, A. Akriche, Structural, mechanical, electronic and thermal properties of  $\text{KZnF}_3$  and  $\text{AgZnF}_3$  Perovskites: FP-(L) APW+ lo calculations, *Solid State Sci.* 58 (2016) 1–13.
- [51] H. Remy, F. Hansen, Röntgenographische Untersuchung des Systems  $\text{KF-MgF}_2$ , *Z. Anorg. Allg. Chem.* 283 (1–6) (1956) 277–286.
- [52] J. Lee, H. Shin, J. Lee, H. Chung, Q. Zhang, F. Saito, Mechanochemical syntheses of perovskite  $\text{KM}^{\text{II}}\text{F}_3$  with cubic structure ( $\text{M}^{\text{II}} = \text{Mg, Ca, Mn, Fe, Co, Ni, and Zn}$ , *Mater. Trans.* 44 (7) (2003) 1457–1460.
- [53] C.D. Martin, S. Chaudhuri, C.P. Grey, J.B.A.M. Parise, Effect of A-site cation radius on ordering of  $\text{BX}_6$  octahedra in (K, Na)  $\text{MgF}_3$  perovskite, *Am. Mineral.* 90 (10) (2005) 1522–1533.
- [54] A.A. Mousa, M.S. Abu-Jafar, D. Dahliah, R.M. Shaltaf, J.M. Khalifeh, Investigation of the perovskite  $\text{KSrX}_3$  ( $X = \text{Cl and F}$ ) compounds, examining the optical, elastic, electronic and structural properties: FP-LAPW study, *J. Electron. Mater.* 47 (1) (2018) 641–650.
- [55] J.P. Poirier, J. Peyronneau, J.-Y. Gesland, G. Brebec, Viscosity and conductivity of the lower mantle-An experimental study on a  $\text{MgSiO}_3$  perovskite analogue,  $\text{KZnF}_3$ , *Phys. Earth Planet. In.* 32 (1983) 273–287.
- [56] O. Muller, R. Roy, *The Major Ternary Structural Families*, Springer-Verlag, Berlin, 1974.
- [57] A.M. Hofmeister, Calculation of bulk modulus and its pressure derivatives from vibrational frequencies and mode Grüneisen Parameters: solids with cubic symmetry or one nearest-neighbor distance, *J. Geophys. Res.: Solid Earth* 96 (B10) (1991) 16181–16203.
- [58] R.A. Heaton, C.C. Lin, Electronic energy-band structure of the  $\text{KMgF}_3$  crystal, *Phys. Rev. B* 25 (6) (1982) 3538.
- [59] G. Murtaza, R. Khenata, M.N. Khalid, S. Naeem, Elastic and optoelectronic properties of  $\text{RbMF}_3$  ( $M = \text{Zn, Cd, Hg}$ ): a mBJ density functional calculation, *Phys. B Condens. Matter* 410 (2013) 131–136.
- [60] A. Gani, O. Cheref, M. Ghezali, M. Rabah, A.H. Reshak, Y. Djaballah, H. Righi, D. Rached, A. Belasri, Mechanical stability and optoelectronic behavior of  $\text{BeXP}_2$  ( $X = \text{Si and Ge}$ ) Chalcopyrite, *Chin. J. Phys.* 64 (2020) 174–182, <https://doi.org/10.1016/j.cjph.2020.01.007>.
- [61] L. Boumia, F. Dahmane, B. Doumi, D.P. Rai, Shakeel A. Khandy, H. Khachai, H. Meradji, Ali H. Reshak, R. Khenata, Structural, electronic and magnetic properties of new full Heusler alloys  $\text{Rh}_2\text{CrZ}$  ( $Z = \text{Al, Ga, In}$ ): first-principles calculations, *Chin. J. Phys.* 59 (2019) 281–290.
- [62] K. Bougherara, D.P. Rai, A.H. Reshak, First principles prediction of the elastic, electronic and optical properties of  $\text{Sn}_3\text{X}_4$  ( $X = \text{P, As, Sb, Bi}$ ) compounds: potential photovoltaic absorbers, *Chin. J. Phys.* 59 (2019) 265–272.